

# Galaxy and Mass Assembly (GAMA): survey diagnostics and core data release

S.P.Driver<sup>1\*</sup>, D.T.Hill<sup>1</sup>, L.S.Kelvin<sup>1</sup>, A.S.G.Robotham<sup>1</sup>, J.Liske<sup>2</sup>, P.Norberg<sup>3</sup>, I.K.Baldry<sup>4</sup>, S.P.Bamford<sup>5</sup>, A.M.Hopkins<sup>6</sup>, J.Loveday<sup>7</sup>, J.A.Peacock<sup>3</sup>, E.Andrae<sup>8</sup>, J.Bland-Hawthorn<sup>9</sup>, S.Brough<sup>6</sup>, M.J.I.Brown<sup>10</sup>, E.Cameron<sup>11</sup>, J.H.Y.Ching<sup>9</sup>, M.Colless<sup>6</sup>, C.J.Conselice<sup>5</sup>, S.M.Croom<sup>9</sup>, N.J.G.Cross<sup>3</sup>, R.De Propriis<sup>12</sup>, S.Dye<sup>13</sup>, M.J.Drinkwater<sup>14</sup>, S.Ellis<sup>9</sup>, Alister W.Graham<sup>15</sup>, M.W.Grootes<sup>15</sup>, M.Gunawardhana<sup>8</sup>, D.H.Jones<sup>6</sup>, E.van Kampen<sup>2</sup>, C.Maraston<sup>12</sup>, R.C.Nichol<sup>16</sup>, H.R.Parkinson<sup>3</sup>, S.Phillipps<sup>17</sup>, K.Pimblet<sup>10</sup>, C.C.Popescu<sup>18</sup>, M.Prescott<sup>4</sup>, I.G.Roseboom<sup>7</sup>, E.M.Sadler<sup>9</sup>, A.E.Sansom<sup>18</sup>, R.G.Sharp<sup>6</sup>, D.J.B.Smith<sup>5</sup>, E.Taylor<sup>8,20</sup>, D.Thomas<sup>16</sup>, R.J.Tuffs<sup>8</sup>, D.Wijesinghe<sup>9</sup>, L.Dunne<sup>5</sup>, C.S.Frenk<sup>22</sup>, M.J.Jarvis<sup>23</sup>, B.F.Madore<sup>24</sup>, M.J.Meyer<sup>25</sup>, M.Seibert<sup>24</sup>, L.Staveley-Smith<sup>25</sup>, W.J.Sutherland<sup>26</sup>, S.J.Warren<sup>27</sup>

<sup>1</sup> School of Physics & Astronomy, University of St Andrews, North Haugh, St Andrews, KY16 9SS, UK; SUPA

<sup>2</sup> European Southern Observatory, Karl-Schwarzschild-Str. 2, 85748, Garching, Germany

<sup>3</sup> Institute for Astronomy, University of Edinburgh, Royal Observatory, Blackford Hill, Edinburgh, EH9 3HJ, UK

<sup>4</sup> Astrophysics Research Institute, Liverpool John Moores University, Twelve Quays House, Egerton Wharf, Birkenhead, CH4 1LD, UK

<sup>5</sup> Centre for Astronomy and Particle Theory, University of Nottingham, University Park, Nottingham, NG7 2RD, UK

<sup>6</sup> Australian Astronomical Observatory, PO Box 296, Epping, NSW 1710, Australia

<sup>7</sup> Astronomy Centre, University of Sussex, Falmer, Brighton, BN1 9QH, UK

<sup>8</sup> Max-Planck Institute for Nuclear Physics (MPIK), Saupfercheckweg 1, 69117 Heidelberg, Germany

<sup>9</sup> Sydney Institute for Astronomy, School of Physics, University of Sydney, NSW 2006, Australia

<sup>10</sup> School of Physics, Monash University, Clayton, Victoria 3800, Australia

<sup>11</sup> Department of Physics, Swiss Federal Institute of Technology (ETH-Zürich), 8093 Zürich, Switzerland

<sup>12</sup> Cerro Tololo Inter-American Observatory, La Serena, Chile

<sup>13</sup> School of Physics and Astronomy, Cardiff University, Queens Buildings, The Parade, Cardiff, CF24 3AA, UK

<sup>14</sup> Department of Physics, University of Queensland, Brisbane, Queensland 4072, Australia

<sup>15</sup> Centre for Astrophysics and Supercomputing, Swinburne University of Technology, Hawthorn, Victoria 3122, Australia

<sup>16</sup> Institute of Cosmology and Gravitation (ICG), University of Portsmouth, Dennis Sciama Building Road, Portsmouth, PO1 3FX, UK

<sup>17</sup> Astrophysics Group, H.H. Wills Physics Laboratory, University of Bristol, Tyndall Avenue, Bristol BS8 1TL, UK

<sup>18</sup> Jeremiah Horrocks Institute, University of Central Lancashire, Preston, PR1 2HE, UK

<sup>19</sup> Instituto Astronomico e Geofisico, University of San Paulo, Brazil

<sup>20</sup> School of Physics, University of Melbourne, Victoria 3010, Australia

<sup>21</sup> Institute for Computational Cosmology, Department of Physics, University of Durham South Road, Durham, DH1 3LE, UK

<sup>22</sup> Centre for Astrophysics, Science & Technology Research Institute, University of Hertfordshire, Hatfield, AL10 9AB, UK

<sup>23</sup> Observatories of the Carnegie Institute of Washington, 813 Santa Barbara Street, Pasadena, CA91101, USA

<sup>24</sup> International Centre for Radio Astronomy Research, The University of Western Australia, 35 Stirling Hwy, Crawley, WA 6009, Australia

<sup>25</sup> Astronomy Unit, Queen Mary University London, Mile End Road, London, E1 4NS, UK

<sup>26</sup> Astrophysics Group, Imperial College London, Blackett Laboratory, Prince Consort Road, London, SW7 2AZ, UK

23 October 2018

## ABSTRACT

The Galaxy And Mass Assembly (GAMA) survey has been operating since February 2008 on the 3.9-m Anglo-Australian Telescope using the AAOmega fibre-fed spectrograph facility to acquire spectra with a resolution of  $R \approx 1300$  for 120 862 SDSS selected galaxies. The target catalogue constitutes three contiguous equatorial regions centred at  $9^h$  (G09),  $12^h$  (G12) and  $14.5^h$  (G15) each of  $12 \times 4 \text{ deg}^2$  to limiting fluxes of  $r_{\text{pet}} < 19.4$ ,  $r_{\text{pet}} < 19.8$ , and  $r_{\text{pet}} < 19.4$  mag respectively (and additional limits at other wavelengths). Spectra and reliable redshifts have been acquired for over 98 per cent of the galaxies within these limits. Here we present the survey footprint, progression, data reduction, redshifting, re-redshifting, an assessment of data quality after 3 years, additional image analysis products (including *ugrizYJHK* photometry, Sérsic profiles and photometric redshifts), observing mask, and construction of our core survey catalogue (GamaCore). From this we create three science ready catalogues: GamaCoreDR1 for public release, which includes data acquired during year 1 of operations within specified magnitude limits (February 2008 to April 2008); GamaCoreMainSurvey containing all data above our survey limits for use by the GAMA team and collaborators; and GamaCoreAtlasSv containing year 1, 2 and 3 data matched to Herschel-ATLAS Science Demonstration data. These catalogues along with the associated spectra, stamps, and profiles, can be accessed via the GAMA website: <http://www.gama-survey.org/>

## 1 INTRODUCTION

Large scale surveys are now a familiar part of the astronomy landscape and assist in facilitating a wide range of science programmes. Three of the most notable wide-area surveys in recent times, with a focus on galactic and galaxy evolution, are the 2 Micron All Sky Survey (2MASS; Skrutskie et al. 2006), the 2 degree Field Galaxy Redshift Survey (2dFGRS; Colless et al. 2001; 2003), and the Sloan Digital Sky Survey (SDSS; York et al. 2000). These surveys have each been responsible for a wide range of science advances attested by their publication and citation records (Trimble & Ceja 2010), ranging from: the identification of new stellar types (e.g., Kirkpatrick et al., 1999); tidal streams in the Galactic Halo (e.g., Belokurov et al. 2006); new populations of dwarf galaxies (e.g., Willman et al. 2005); galaxy population statistics (e.g., Bell et al. 2003; Baldry et al. 2006); the recent cosmic star-formation history (e.g., Heavens et al. 2004); group catalogues (e.g., Eke et al. 2004); merger rates (e.g., Bell et al., 2006); quantification of large scale structure (e.g., Percival et al. 2001); galaxy clustering (e.g., Norberg et al. 2001); and, in conjunction with CMB and SNIa searches, convergence towards the basic cosmological model now adopted as standard (e.g., Spergel et al. 2003; Cole et al. 2005). In addition to these mega-surveys there have been a series of smaller, more specialised, local surveys including the Millennium Galaxy Catalogue (MGC; Driver et al., 2005), the 6dF Galaxy Survey (6dFGS; Jones et al. 2004, 2009), the HI Parkes All Sky Survey (HIPASS; Meyer et al. 2004), and the Galaxy Evolution Explorer (GALEX; Martin et al. 2005) mission, which are each opening up new avenues of extra-galactic exploration (i.e., structural properties, the near-IR domain, the 21cm domain, and the UV domain respectively). Together these surveys provide an inhomogeneous nearby reference point for the very narrow high- $z$  pencil beam surveys underway (i.e., DEEP2, VVDS, COSMOS, GEMS etc.), and from which comparative studies can be made to quantify the process of galaxy evolution (e.g., Cameron & Driver 2007).

The Galaxy And Mass Assembly Survey (GAMA) has been established with two main sets of aims, which are surveyed in Driver et al. (2009). The first is to use the galaxy distribution to conduct a series of tests of the Cold Dark Matter (CDM) paradigm, and the second is to carry out detailed studies of the internal structure and evolution of the galaxies themselves.

The CDM model is now the standard means by which data relevant to galaxy formation and evolution are interpreted, and it has met with great success on 10–100 Mpc scales. The next challenge in validating this standard model is to move beyond small linear fluctuations, into the regime dominated by dark-matter haloes. The fragmentation of the dark matter into these roughly spherical virialized objects is robustly predicted both numerically and analytically over seven orders of magnitude in halo mass (e.g., Springel et al. 2005). Massive haloes are readily identified as rich clusters of galaxies, but it remains a challenge to probe further down the mass function. For this purpose, one needs to identify low-mass groups of galaxies, requiring a survey that probes far down the galaxy luminosity function over a large representative volume. But having found low-mass haloes, the galaxy population within each halo depends critically on the

interaction between the baryon processes (i.e., star formation rate and feedback efficiency) and the total halo mass. In fact the ratio of stellar mass to halo mass is predicted (Bower et al. 2006; De Lucia et al. 2006) to be strongly dependent on halo mass, exhibiting a characteristic dip at Local Group masses. The need for feedback mechanisms to suppress star formation in both low mass haloes (via supernovae) and high mass haloes (via AGN) is now part of standard prescriptions in modeling galaxy formation. With GAMA we can connect these theoretical ingredients directly with observational measurements.

However, the astrophysics of galaxy bias is not the only poorly understood area in the CDM model. Existing successes have been achieved at the price of introducing Dark Energy as the majority constituent of the Universe, and a key task for cosmology is to discriminate between various explanations for this phenomenon: a cosmological constant, time varying scalar field, or a deficiency in our gravity model. These aspects can be probed by GAMA in two distinct ways: either the form or evolution of the halo mass function may diverge from standard predictions of gravitational collapse in the highly nonlinear regime, or information on non-standard models may be obtained from velocity fields on 10-Mpc scales. The latter induce redshift-space anisotropies in the clustering pattern, which measure the growth rate of cosmic structure (e.g., Guzzo et al. 2008). Thus GAMA has the potential to illuminate both the astrophysical and fundamental aspects of the CDM model.

Moving beyond the large-scale distribution, GAMA's main long-term legacy will be to create a uniform galaxy database, which builds on earlier local surveys in a comprehensive manner to fainter flux levels, higher redshift, higher spatial resolution, and spanning UV to radio wavelengths. The need for a combined homogeneous, multiwavelength, and spatially resolved study can be highlighted by three topical issues:

1. **Galaxy Structure.** Galaxies are typically comprised of bulge and/or disc components that exhibit distinct properties (dynamics, ages, metallicities, profiles, dust and gas content), indicating potentially distinct evolutionary paths (e.g., cold smooth and hot lumpy accretion; cf. Driver et al. 2006 or Cook et al. 2010). This is corroborated by the existence of the many SMBH-bulge relations (see, for example, Novak, Faber & Dekel 2006), which firmly couples spheroidal evolution with AGN history (Hopkins et al. 2006). A comprehensive insight into galaxy formation and evolution therefore demands consideration of the structural components requiring high spatial resolution imaging on  $\sim 1$  kpc scales or better (e.g., Allen et al. 2006; Gadotti 2009).

2. **Dust attenuation.** A recent spate of papers (Shao et al. 2007; Choi et al. 2007; Driver et al. 2007, 2008; Masters et al. 2010) have highlighted the severe impact of dust attenuation on the measurement of basic galaxy properties (e.g., fluxes and sizes). In particular, dust attenuation is highly dependent on wavelength, inclination, and galaxy type with the possibility of some further dependence on environment. Constructing detailed models for the attenuation of stellar light by dust in galaxies and subsequent re-emission (e.g., Popescu et al. 2000), is intractable without extensive wavelength coverage extending from the UV through to the far-IR. To survey the dust content for a significant sample of galaxies therefore demands a multi-wavelength dataset ex-

tending over a sufficiently large volume to span all environments and galaxy types. The GAMA regions are or will be surveyed by the broader GALEX Medium Imaging Survey and Herschel-ATLAS (Eales et al. 2010) programmes, providing UV to FIR coverage for a significant fraction of our survey area.

**3. The HI content.** As star-formation is ultimately driven by a galaxy’s HI content any model of galaxy formation and evolution must be consistent with the observed HI properties (see for example discussion in Hopkins, McClure-Griffiths & Gaensler 2008). Until recently probing HI beyond very low redshifts has been laborious if not impossible due to ground-based interference and/or sensitivity limitations (see for example Lah et al. 2009). The new generation of radio arrays and receivers are using radio-frequency interference mitigation methods coupled with new technology receivers to open up the HI Universe at all redshifts (i.e., ASKAP, MeerKAT, LOFAR, and ultimately the SKA). This will enable coherent radio surveys that are well matched in terms of sensitivity and resolution to optical/near-IR data. Initial design study investment has been made in the DINGO project, which aims to conduct deep HI observations within a significant fraction of the GAMA regions using ASKAP (Johnston et al. 2007).

The GAMA survey will eventually provide a wide-area highly complete spectroscopic survey of over 400k galaxies with sub-arcsecond optical/near-IR imaging (SDSS/UKIDSS/VST/VISTA). Complementary multi-wavelength photometry from the UV (GALEX), mid-IR (WISE) and far-IR (Herschel) and radio wavelengths (ASKAP, GMRT) is being obtained by a number of independent public and private survey programmes. These additional data will ultimately be ingested into the GAMA database as they become available to the GAMA team. At the heart of the survey is the 3.9-m Anglo Australian Telescope (AAT), which is being used to provide the vital distance information for all galaxies above well specified flux, size and isophotal detection limits. In addition the spectra from AAOmega for many of the sample will be of sufficiently high signal-to-noise and spectral resolution ( $\approx 3 - 6 \text{ \AA}$ ) to allow for the extraction of line diagnostic information leading to constraints on star-formation rates, velocity dispersions and other formation/evolutionary markers. The area and depth of GAMA compared to other notable surveys is detailed in Baldry et al. (2010; their Fig. 1). In general GAMA lies in the parameter space between that occupied by the very wide shallow surveys and the deep pencil beam surveys and is optimised to study structure on  $\sim 10 h^{-1} \text{ Mpc}$  to  $1 h^{-1} \text{ kpc}$  scales, as well as sample the galaxy population from FUV to radio wavelengths.

This paper describes the first three years of the GAMA AAOmega spectroscopic campaign, which has resulted in 112k new redshifts (in addition to the 19k already known in these regions). In section 2 we describe the spectroscopic progress, data reduction, redshifting, re-redshifting, an assessment of the redshift accuracy and blunder rate, and an update to our initial visual classifications. In section 3 we describe additional image analysis resulting in *ugrizYJHK* matched aperture photometry, Sérsic profiles, and photometric redshifts. In section 4 we describe the combination of the data presented in section 2 and 3 to form our core catalogue and investigate the completeness versus magnitude,

colour, surface brightness, concentration, and close pairs. In section 5 we present the survey masks required for spatial clustering studies and in section 6 present our publicly available science ready catalogue. These catalogues along with an MySQL tool and other data inspection tools are now available at: <http://www.gama-survey.org/> and we expect future releases of redshifts and other data products to occur on an approximately annual cycle.

Please note all magnitudes used in this paper, unless otherwise specified, are  $r$ -band Petrosian ( $r_{\text{pet}}$ ) from SDSS DR6, which have been extinction corrected and placed onto the true AB scale following the prescription described by the SDSS DR6 release (Adelman-McCarthy et al. 2008).

## 2 THE GAMA AAT SPECTROSCOPIC SURVEY

### 2.1 GAMA field selection, input catalogue and tiling algorithm

The initial GAMA survey consists of three equatorial regions, each of  $12 \times 4 \text{ deg}^2$  (see Table 1 and Fig. 1). The decision for this configuration was driven by three considerations: suitability for large-scale structure studies demanding contiguous regions of  $\sim 50 \text{ deg}^2$  to fully sample  $\sim 100$  co-moving  $h^{-1} \text{ Mpc}$  structures at  $z \approx 0.2$ ; observability demanding a 5 hr Right Ascension baseline to fill a night’s worth of observations over several lunations; and overlap with existing and planned surveys, in particular the SDSS (York et al. 2000), UKIDSS LAS (Lawrence et al. 2007), VST KIDS, VISTA VIKING, H-ATLAS (Eales et al. 2010), and ASKAP DINGO. Fig. 1 shows the overlap of some of these surveys. Note the H-ATLAS SGP survey region has changed since Fig. 5 of Driver et al. (2009) due to additional space-craft limitations introduced in-flight. The depth and area of the GAMA AAT spectroscopic survey were optimised following detailed simulations of the GAMA primary science goal of measuring the Halo Mass Function. This resulted in an initial survey area of  $144 \text{ deg}^2$  to a depth of  $r_{\text{pet}} < 19.4$  mag in the  $9^h$  and  $15^h$  regions and an increased depth of  $r_{\text{pet}} < 19.8$  mag in the  $12^h$  region (see Table 1). In addition for year 2 and 3 observations additional  $K$  and  $z$ -band selection was introduced such that the final main galaxy sample (Main Survey) can be defined (see Baldry et al., 2010) as follows:

**G09:**  $r_{\text{pet}} < 19.4$  OR ( $K_{\text{Kron}} < 17.6$  AND  $r_{\text{model}} < 20.5$ ) OR ( $z_{\text{model}} < 18.2$  AND  $r_{\text{model}} < 20.5$ ) mag

**G12:**  $r_{\text{pet}} < 19.8$  OR ( $K_{\text{Kron}} < 17.6$  AND  $r_{\text{model}} < 20.5$ ) OR ( $z_{\text{model}} < 18.2$  AND  $r_{\text{model}} < 20.5$ ) mag

**G15:**  $r_{\text{pet}} < 19.4$  OR ( $K_{\text{Kron}} < 17.6$  AND  $r_{\text{model}} < 20.5$ ) OR ( $z_{\text{model}} < 18.2$  AND  $r_{\text{model}} < 20.5$ ) mag

with all magnitudes expressed in AB. For the remainder of this paper we mainly focus, for clarity, on the  $r$ -band selected data and note that equivalent diagnostic plots to those shown later in this paper can easily be created for the  $z$  and  $K$  selections.

**Table 1.** Coordinates of the three GAMA equatorial fields.

| Field | RA(J2000 deg.) | Dec(J2000 deg.) | Area (deg <sup>2</sup> ) | Depth (mag)             |
|-------|----------------|-----------------|--------------------------|-------------------------|
| G09   | 129.0...141.0  | +3.0... - 1.0   | 12 × 4                   | $r_{\text{pet}} < 19.4$ |
| G12   | 174.0...186.0  | +2.0... - 2.0   | 12 × 4                   | $r_{\text{pet}} < 19.8$ |
| G15   | 211.5...223.5  | +2.0... - 2.0   | 12 × 4                   | $r_{\text{pet}} < 19.4$ |

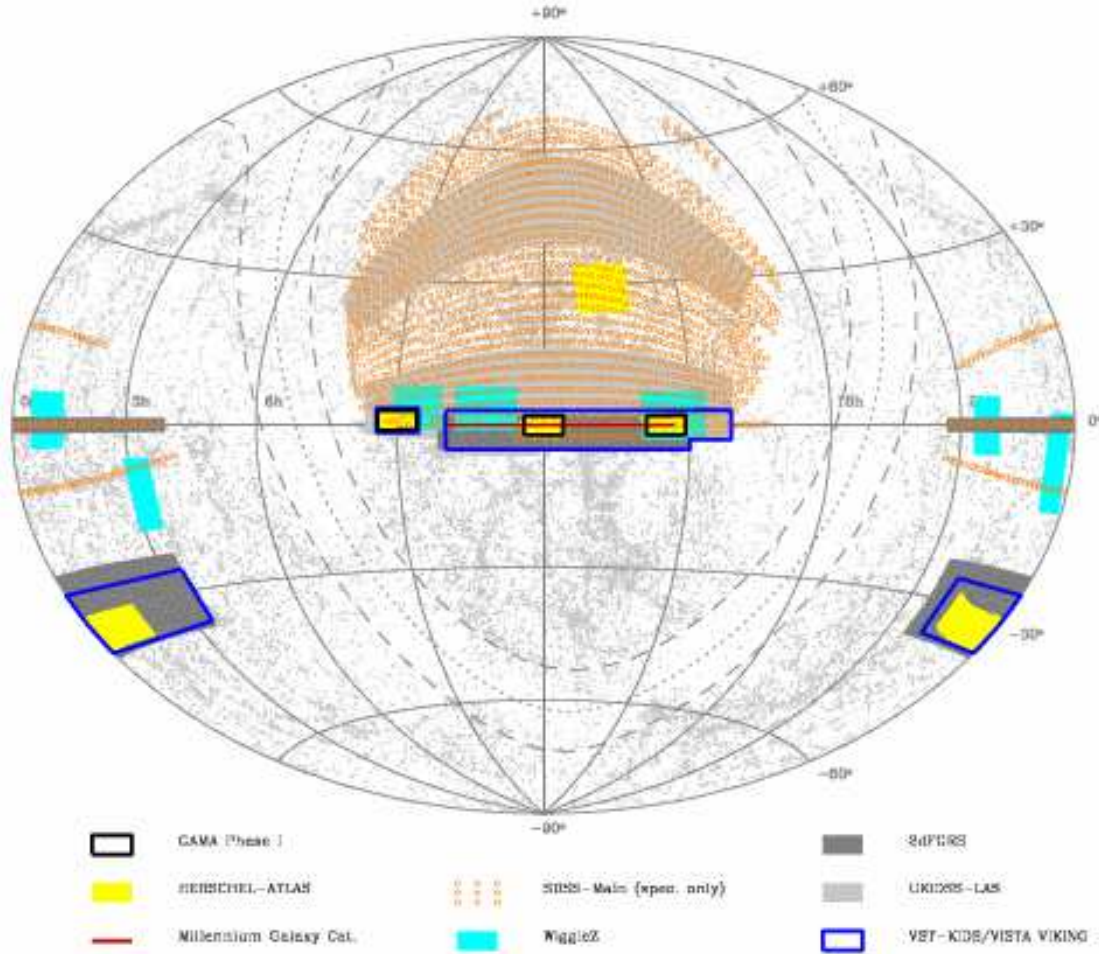


**Figure 1.** GAMA Phase I (black squares) in relation to other recent and planned surveys (see key). For a zoom in to the GAMA regions showing SDSS, UKIDSS and GALEX overlap please see Fig. 1 of the companion paper describing the photometry by Hill et al., (2010a). Also overlaid as grey dots are all known redshifts at  $z < 0.1$  taken from NASA ExtraGalactic Database.

## 2.2 Survey preparation

The input catalogue for the GAMA spectroscopic survey was constructed from SDSS DR6 (Adelman-McCarthy et al. 2008) and our own reanalysis of UKIDSS LAS DR4 (Lawrence et al. 2007) to assist in star-galaxy separation; see Hill et al. (2010a) for details. The preparation of the input catalogue, including extensive visual checks and the revised star-galaxy separation algorithm, is described and assessed in detail by Baldry et al. (2010). The survey is being conducted using the AAT’s AAOmega spectrograph system (an

upgrade of the original 2dF spectrographs: Lewis et al. 2002; Sharp et al. 2006).

In year 1 we implemented a uniform grid tiling algorithm (see Fig. 2, upper panels), which created a significant imprint of the tile positions on the spatial completeness distribution. Subsequently, for years 2 and 3 we implemented a heuristic “greedy” tiling strategy, which was designed to maximise the spatial completeness across the survey regions within 0.14 deg smoothed regions. Full details of the GAMA science requirements and the tiling strategy devised to meet these are laid out by Robotham et al. (2010). The efficiency

of this strategy is discussed further in section 5. The final location of all tiles is shown in Fig. 2 and the location of objects for which redshifts were not secured or not observed are shown in the lower panels of Fig. 3 as black dots or red crosses respectively.

### 2.3 Observations and data reduction

All GAMA 2dF pointings (tiles) were observed during dark or grey time with exposure times mostly ranging from 3000 to 5000 s (in 3 to 5 exposures) depending on seeing and sky brightness. Observations were generally conducted at an hour angle of less than 2 hr (the median zenith distance of the observations is  $35^\circ$ ) and with the Atmospheric Dispersion Corrector engaged. We used the 580V and 385R gratings with central wavelengths of 4800 Å and 7250 Å in the blue and red arms, respectively, separated by a 5700 Å dichroic. This set-up yielded a continuous wavelength coverage of 3720 Å–8850 Å at a resolution of  $\approx 3.5$  Å (in the blue channel) and  $\approx 5.5$  Å (in the red channel). Every block of science exposures was accompanied by a flat-field and an arc-lamp exposure, while a master bias frame was constructed once per observing run. In each observation fibres were allocated to between 318 and 366 galaxy targets (depending on the number of broken fibres), to at least 20 blank sky positions, to 3–5 SDSS spectroscopic standards, and to 6 guide stars selected from the SDSS in the range  $14.35 < r_{\text{pet}} < 14.5$  mag (verified via cross-matching with the USNO-B catalogue to ensure proper motions were below 15 mas/yr). Galaxy targets were prioritised as indicated in Table 1 of Robotham et al. (2010). The location of all 392 tile centres are shown in Fig. 2. The change in tiling strategy from a fixed grid system in year 1 to the greedy tiling strategy in years 2 and 3 is evident with the latter leading to an extremely spatially uniform survey (see section 5). The overall progress of the survey in terms of objects per night and the cumulative total numbers are shown in Fig. 4 illustrating that typically between 1500 and 2500 redshifts were obtained per night over the three year campaign.

The data were reduced at the telescope in real time using the (former<sup>1</sup>) Anglo-Australian Observatory’s 2dfdr software (Croom, Saunders & Heald 2004) developed continuously since the advent of 2dF, and recently optimised for AAOmega. The software is described in a number of AAO documents<sup>2</sup>. Briefly, it performs automated tramline detection, sky subtraction, wavelength calibration, stacking and splicing. Following the standard data reduction we attempted to improve the sky subtraction by applying a principal component analysis (PCA) technique similar to that described by Wild & Hewett (2005) and described in detail by Sharp & Parkinson (2010). We note that  $\sim 5$  per cent of all spectra are affected by fringing (caused by small air gaps between the adhesive that joins a fibre with its prism), and we are currently studying algorithms that might remove or at least mitigate this effect.

<sup>1</sup> Note that from 1st July 2010 the Anglo Australian Observatory (AAO) has been renamed the Australian Astronomical Observatory (AAO), see Watson & Colless (2010).

<sup>2</sup> [http://www.aao.gov.au/AAO/2df/aaomega/aaomega\\_software.html](http://www.aao.gov.au/AAO/2df/aaomega/aaomega_software.html)

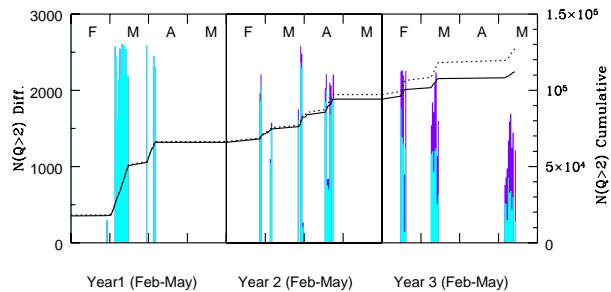


**Figure 4.** Progression of the GAMA survey in terms of spectra and redshift acquisition for years 1, 2 and 3 as indicated. The cyan line shows the number of spectra obtained per night within our main survey limits, mauve shows the number below our flux limits (i.e., secondary targets and fillers). The solid line shows the cumulative distribution of redshifts within our survey limits and the dashed line shows the cumulative distribution of all redshifts. The cumulative distributions include pre-existing redshifts and are calculated monthly rather than nightly.

### 2.4 Redshifting

The fully reduced and PCA-sky-subtracted spectra were initially redshifted by the observers at the telescope using the code RUNZ, which was originally developed by Will Sutherland for the 2dFGRS (now maintained by Scott Croom). RUNZ attempts to determine a spectrum’s redshift (i) by cross-correlating it with a range of templates, including star-forming, E+A and quiescent galaxies; A, O and M stars; as well as QSO templates; (ii) by fitting Gaussians to emission lines and searching for multi-line matches. These estimates are quasi-independent because the strongest emission lines are clipped from the templates before the cross-correlation is performed. RUNZ then proceeds by presenting its operator with a plot of the spectrum marking the positions of common nebular emission and stellar absorption lines at the best automatic redshift. This redshift is then checked visually by the operator who, if it is deemed incorrect, may use a number of methods to try to find the correct one. The process is concluded by the operator assigning a (subjective) quality ( $Q$ ) to the finally chosen redshift:

- $Q = 4$ : The redshift is certainly correct.
- $Q = 3$ : The redshift is probably correct.
- $Q = 2$ : The redshift may be correct. Must be checked before being included in scientific analysis.
- $Q = 1$ : No redshift could be found.
- $Q = 0$ : Complete data reduction failure.

With the above definitions it is understood that by assigning  $Q \geq 3$  a redshift is approved as suitable for inclusion in scientific analysis. Note that  $Q$  refers to the (subjective) quality of the *redshift*, not of the *spectrum*.

### 2.5 Re-redshifting

The outcome of the redshifting process described above will not be 100 per cent accurate. It is inevitable that some fraction of the  $Q \geq 3$  redshifts will be incorrect. Furthermore, the quality assigned to a redshift is somewhat subjective and

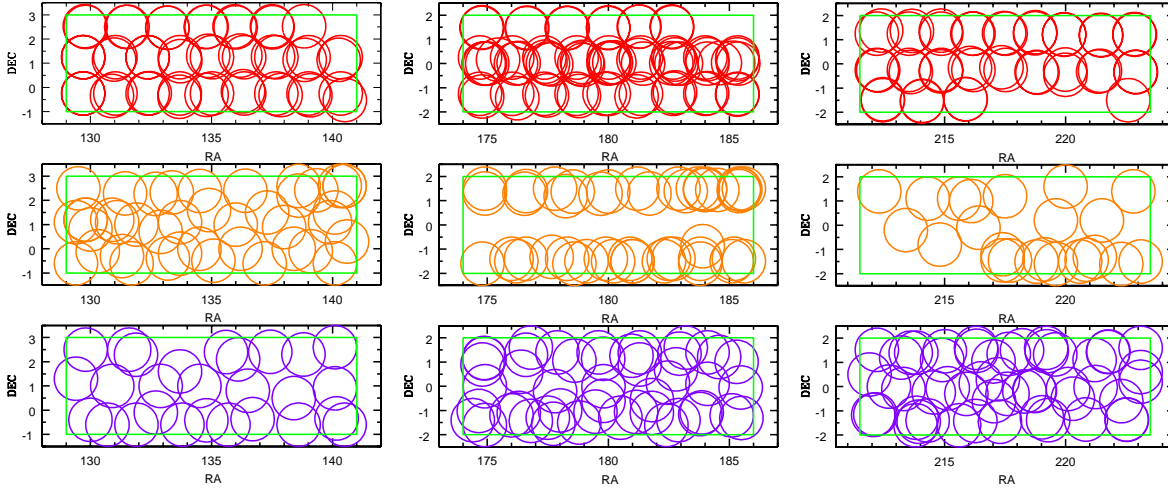


**Figure 2.** Location of the tiles in year 1 (top), year 2 (centre), and year 3 (bottom) and for G09 (left), G12 (centre) and G15 (right).

will depend on the experience of the redshifter. In an effort to weed out mistakes, to quantify the probability of a redshift being correct, and thereby to homogenise the quality scale of our redshifts, a significant fraction of our sample has been independently re-redshifted. This process and its results will be described in detail by Liske et al. (2010, in prep.). Briefly, the spectra of all  $Q = 2$  and 3 redshifts, of all  $Q = 4$  redshifts with discrepant photo- $z$ 's, and of an additional random  $Q = 4$  sample have been independently re-redshifted, where those conducting the re-redshifting had no knowledge of the originally assigned redshift or  $Q$ . The  $Q = 2$  sample was re-examined twice. Overall approximately one third of the entire GAMA sample was re-evaluated. The results of the blind re-redshifting process were used to estimate the probability, for each redshifter, that she/he finds the correct redshift as a function of  $Q$  (for  $Q \geq 2$ ), or that she/he has correctly assigned  $Q = 1$ . Given these probabilities, and given the set of redshift “opinions” for a spectrum, we have calculated for each redshift found for this spectrum the probability,  $p_z$ , that it is correct. This allowed us to select the “best” redshift in cases where more than one redshift had been found for a given spectrum. It also allowed us to construct a “normalised” quality scale:

$$\begin{aligned} nQ &= 4 \text{ if } p_z \geq 0.95 \\ nQ &= 3 \text{ if } 0.9 \leq p_z < 0.95 \\ nQ &= 2 \text{ if } p_z < 0.9 \\ nQ &= 1 \text{ if it is not possible to measure a redshift from this spectrum.} \end{aligned}$$

Unlike  $Q$ , whose precise, quantitative meaning depends on the redshifter who assigned it, the meaning of  $nQ$  is homogeneous across the entire redshift sample.

In Fig. 5 we show one example each of a spectrum with  $nQ = 4$ ,  $nQ = 3$  and  $nQ = 2$ .

## 2.6 Final redshift sample

In the three years of observation completed so far we have observed 392 tiles, resulting in 135 902 spectra in total

(including standard stars), and 134 390 spectra of 120 862 unique galaxy targets. Of these, 114 043 have a reliable redshift with  $nQ \geq 3$ , implying a mean overall redshift completeness of 94.4 per cent. Restricting the sample to the  $r$ -limited Main Survey targets (i.e., ignoring the  $K$  and  $z$  selection and fainter fillers), we find that the completeness is  $> 98$  per cent in all three GAMA regions, leaving little room for any severe spectroscopic bias. Fig. 6 shows the evolution of the survey completeness for the main  $r$ -band limited sample versus apparent magnitude across (left-to-right) the three GAMA regions.

## 2.7 Redshift accuracy and reliability

Quantifying the redshift accuracy and blunder rate is crucial for most science applications and can be approached in a number of ways. Here we compare redshifts obtained for systems via repeat observations within GAMA (Intra-GAMA comparison) and also repeat observations of objects surveyed by earlier studies (Inter-survey comparison).

### 2.7.1 Intra-GAMA comparison

Our sample includes 974 objects that were observed more than once and for which we have more than one  $nQ \geq 3$  redshift from independent spectra. The distribution of pairwise velocity differences,  $\Delta v$ , of this sample is shown as the shaded histogram in the left panel of Fig. 7. This distribution is clearly not Gaussian but roughly Lorentzian (blue line), although with a narrower core, and there are a number of outliers (see below). Nevertheless, if we clip this distribution at  $\pm 500 \text{ km s}^{-1}$  we find a 68-percentile range of  $185 \text{ km s}^{-1}$ , indicating a redshift error  $\sigma_v = 65 \text{ km s}^{-1}$ . However, this value is likely to depend on  $nQ$ . Indeed, if we restrict the sample to pairs where both redshifts have  $nQ = 4$  (red histogram), we find  $\sigma_{v,4} = 60 \text{ km s}^{-1}$ . Our sample of pairs where both redshifts have  $nQ = 3$  is small (22 pairs) but this yields  $\sigma_{v,3} = 101 \text{ km s}^{-1}$ . However, given  $\sigma_{v,4}$  we can also use our larger sample of pairs where one redshift has  $nQ = 3$  and the other has  $nQ = 4$  (green histogram) to

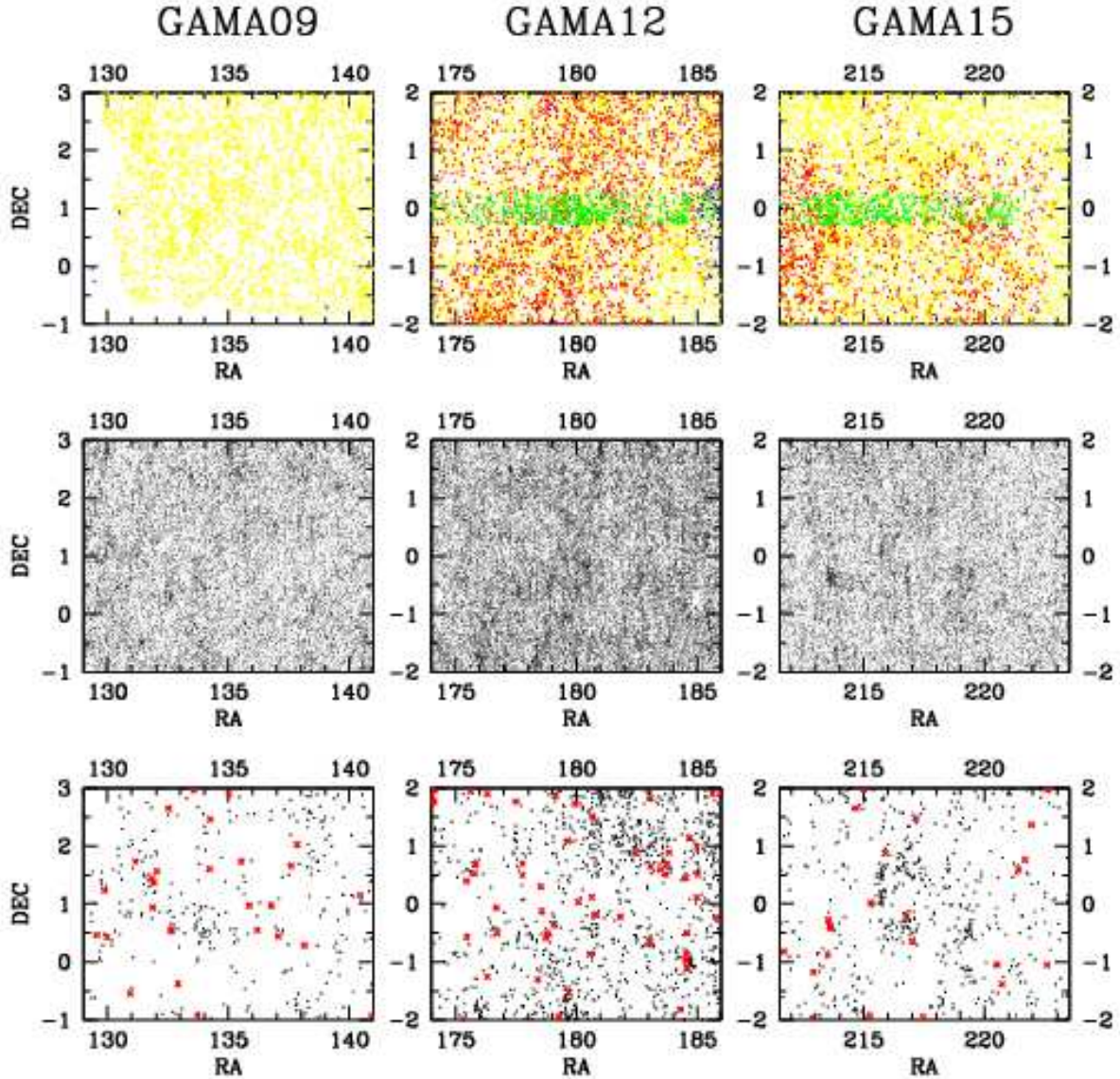


**Figure 3.** (top) The distribution of pre-existing redshifts (SDSS, yellow; 2dFGRS, red; MGC, green; other, blue) within the three regions (as indicated). (middle) the distributions of redshifts acquired during the GAMA Phase I campaign, and (lower) the distribution of targets for which redshifts were not obtained (black dots) or were not targeted (red crosses).

obtain an independent estimate of  $\sigma_{v,3} = 97 \text{ km s}^{-1}$ , which is in reasonable agreement.

Defining discrepant redshift pairs as those with  $|\Delta v| > 500 \text{ km s}^{-1}$ , and assuming that only one, but not both of the redshifts of such pairs is wrong, we find that 3.6 per cent of redshifts with  $nQ = 4$  are in fact wrong. This is in reasonable agreement with the fact that  $nQ = 4$  redshifts are defined as those with  $p_z > 0.95$ . However, for  $nQ = 3$  we find a blunder rate of 15.1 per cent, which is somewhat higher than expected based on the fact that  $nQ = 3$  is defined as  $p_z > 0.9$ . We surmise that this is likely to be the result of a selection effect: many of the objects in this sample are likely to have been re-observed by GAMA because the

initial redshift of the first spectrum was only of a low quality (i.e.  $Q = 2$ ). However, subsequent re-redshifting of the initial spectrum (after the re-observation) may have produced confirmation of the initial redshift, which will have bumped the redshift quality to  $nQ = 3$ . Hence this sample is likely to include many spectra that are of worse quality, and or spectra that are harder to redshift than the average  $nQ = 3$  spectrum, which will produce a higher blunder rate for this sample than the average blunder rate for the whole  $nQ = 3$  sample. Indeed, the median S/N of this sample is 20 per cent lower than for the full GAMA sample. Note that this may also have an effect on the redshift accuracies determined

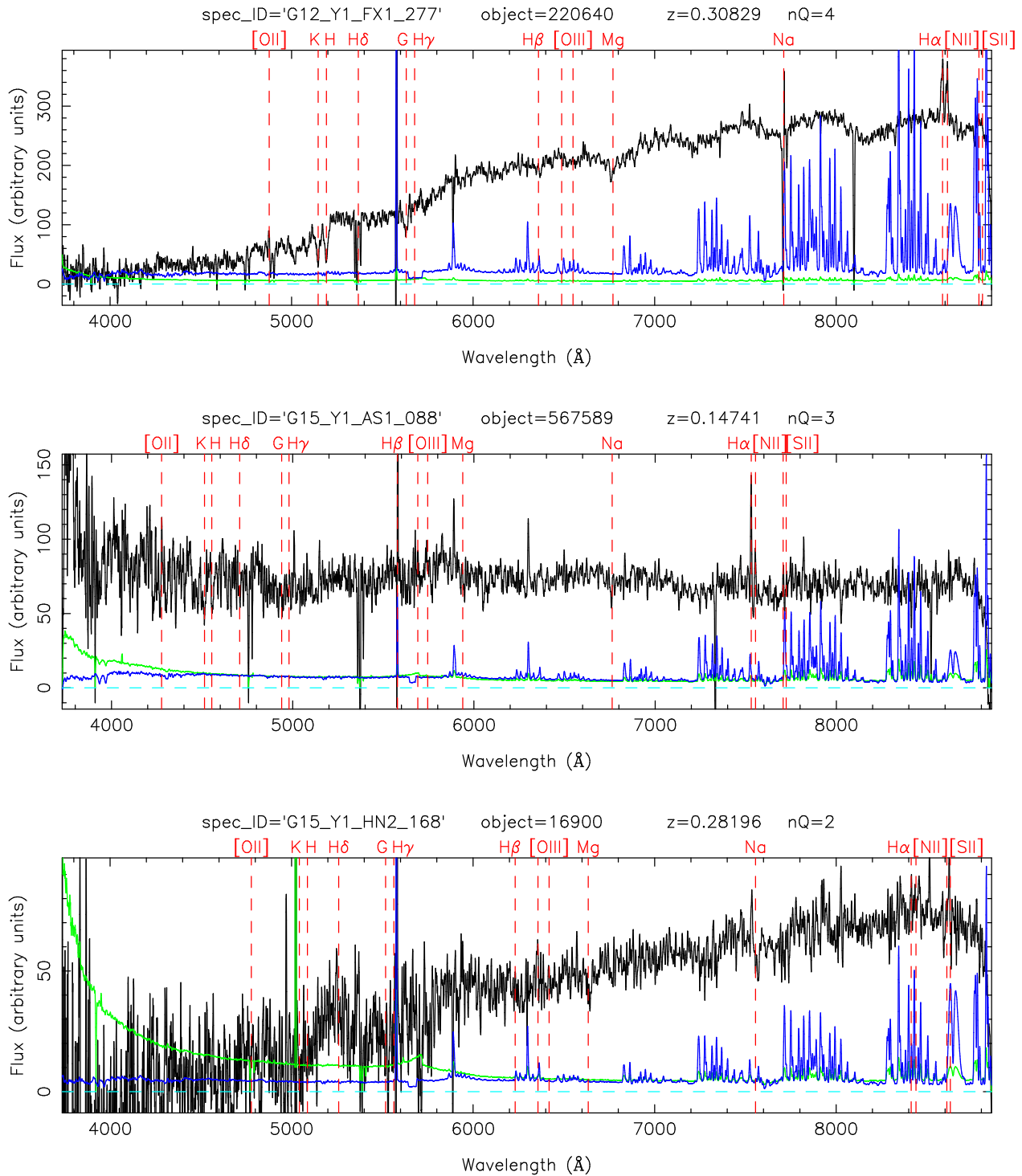


**Figure 5.** Examples of spectra with redshift quality  $nQ = 4$  (top panel), 3 (middle) and 2 (bottom). We show the spectrum (black), the  $1\sigma$  error (green) and the mean sky spectrum (blue, scaled arbitrarily w.r.t. the spectrum). The vertical dashed red lines mark the positions of common nebular emission and stellar absorption lines at the redshift of the galaxy. The spectra were smoothed with a boxcar of width 5 pixels.



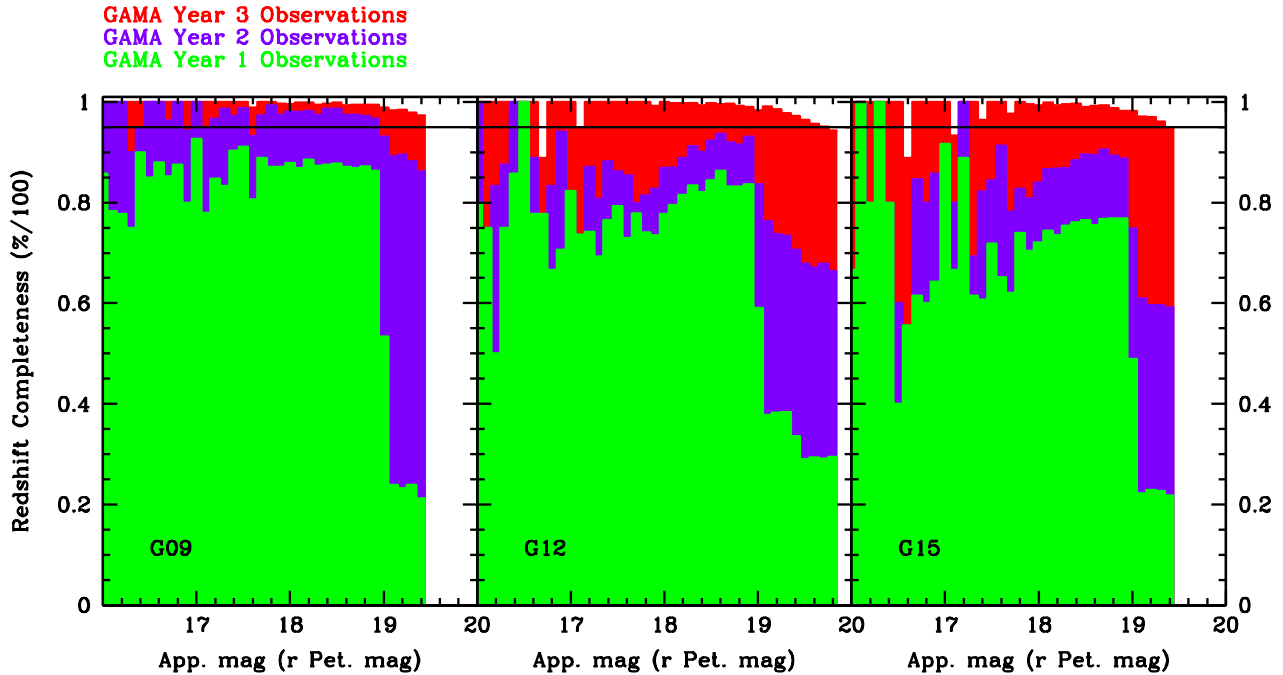


**Figure 6.** Evolution the redshift completeness ( $Q \geq 3$ ) of the GAMA survey (main  $r$ -band selection only) over three years of observations showing the progressive build-up towards uniform high completeness. The horizontal line denotes a uniform 95 per cent completeness.

above. This will be investigated in more detail by Liske et al. (2010, in prep).

### 2.7.2 Inter-survey comparisons

Our sample includes 2522 unique GAMA spectra (with  $nQ \geq 3$  redshifts) for objects that had previously been observed by other surveys (see section 2.8), for a total of 2671 GAMA–non-GAMA pairs. The distribution of the velocity differences of this sample is shown as the shaded histogram in the right panel of Fig. 7. Approximately 81 per cent of the non-GAMA spectra in this sample are from the 2dFGRS and the MGC, which were both obtained with 2dF, using the same set-up and procedures. For the 2dFGRS, Colless et al. (2001) quote an average redshift uncertainty of  $85 \text{ km s}^{-1}$ . Using this value together with the observed 68-percentile ranges of the velocity differences of the GAMA( $nQ = 4, 3$ )–non-GAMA( $nQ \geq 3$ ) sample (red and green histograms, respectively) we find  $\sigma_{v,4} = 51 \text{ km s}^{-1}$  and  $\sigma_{v,3} = 88 \text{ km s}^{-1}$ . These values are somewhat lower than those derived in the previous section. The most likely explanation for this is that the inter-survey sample considered here is brighter than the intra-GAMA sample of the previous section (because of the spectroscopic limits of the 2dFGRS and MGC). Indeed, the median S/N of the GAMA spectra in the inter-survey sample is a factor of 1.7 higher than that of the spectra in the intra-GAMA sample.

As above, we can also attempt to estimate the GAMA blunder rate from the inter-survey sample. From the GAMA( $nQ = 4$ )–non-GAMA( $nQ \geq 3$ ) sample we find a GAMA  $nQ = 4$  blunder rate of 5.0 per cent if we assume that *all* redshift discrepancies are due to GAMA mistakes.

However, this is clearly not the case since the blunder rate improves to 3.0 per cent if we restrict the sample to pairs with  $nQ \geq 4$  non-GAMA redshifts. Similarly, the GAMA  $nQ = 3$  blunder rate comes out at 10.1 or 4.2 per cent depending on whether one includes the pairs with non-GAMA  $nQ = 3$  redshifts or not, considerably lower than the corresponding value derived in the previous section.

In summary, it seems likely that neither the intra-GAMA nor the inter-survey sample are fully representative of the complete GAMA sample. The former is on average of lower quality than the full sample while the latter is of higher quality. Hence we must conclude that the redshift accuracies and blunder rates determined from these samples are not representative either, but are expected to span the true values. A full analysis of these issues will be provided by Liske et al. (2010) following re-redshifting of the recently acquired year 3 data.

### 2.8 Merging GAMA with data from earlier redshift surveys

The GAMA survey builds upon regions of sky already sampled by a number of surveys, most notably the SDSS and 2dFGRS but also several others (as indicated in Table 2). As the GAMA input catalogue (Baldry et al. 2010) has taken the pre-existing redshifts into account, the GAMA data by themselves constitute a highly biased sample missing 80–90 per cent of bright sources with  $r_{\text{pet}} < 17.77$  mag and fainter objects previously selected by AGN or LRG surveys. It is therefore important for almost any scientific application, outside of analysing AAOmega performance, to produce extended catalogues that include both the GAMA and

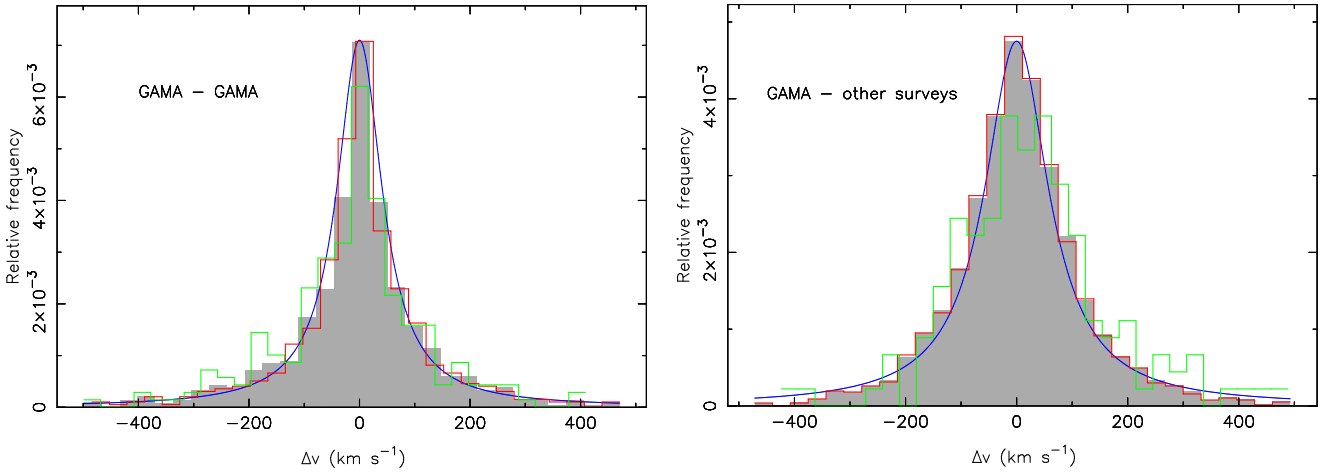


**Figure 7.** Left: The shaded histogram shows the distribution of differences between the redshifts measured from independent GAMA spectra of the same objects, where all redshifts have  $nQ \geq 3$  (868 pairs from 1718 unique spectra of 856 unique objects). The red histogram shows the same for pairs where both redshifts have  $nQ = 4$  (617 pairs from 1216 unique spectra of 605 unique objects). The green histogram shows the same for pairs where one redshift has  $nQ = 3$  and the other  $nQ = 4$  (229 pairs from 458 unique spectra of 229 unique objects). The blue line shows a Lorentzian with  $\gamma = 50 \text{ km s}^{-1}$  for comparison. Right: The shaded histogram shows the distribution of differences between the redshifts measured from independent GAMA and non-GAMA spectra of the same objects, where all redshifts have  $nQ \geq 3$  (2533 pairs from 4892 unique spectra of 2359 unique objects). The red histogram shows the same for pairs where the GAMA redshift has  $nQ = 4$  and the non-GAMA redshift  $nQ \geq 3$  (2385 pairs from 4618 unique spectra of 2233 unique objects). The green histogram shows the same for pairs where the GAMA redshift has  $nQ = 3$  (148 pairs from 290 unique spectra of 142 unique objects). The blue line shows a Lorentzian with  $\gamma = 70 \text{ km s}^{-1}$  for comparison.

pre-GAMA data. Fig. 8 shows the  $n(z)$  distributions of redshifts in the three GAMA blocks to  $r_{\text{pet}} < 19.4$  mag in G09 and G15 and to  $r_{\text{pet}} < 19.8$  mag in G12 colour coded to acknowledge the survey from which they originate. Table 2 shows the contribution to the combined redshift catalogue from the various surveys. Note the numbers shown in Table 2 may disagree with those shown in Baldry et al. (2010) as some repeat observations of previous targets were made.

## 2.9 Update to visual inspection of the input catalogue

The GAMA galaxy target catalogue has been constructed in an automated fashion from the SDSS DR6 (see Baldry et al. 2010) and a number of manual checks of the data based on flux and size ratios and various SDSS flags were made. This resulted in 552 potential targets being expunged from the survey prior to Year 3 (Baldry et al. 2010). Expunged targets were given `VIS_CLASS` values of 2 (no evidence of galaxy light) or 3 (not the main part of a galaxy). In reality, objects with `VIS_CLASS`=3 were targeted but at a lower priority (below the main survey but above any filler targets) with most receiving redshifts by the end of Year 3. About 6 percent of these were, by retrospective visual inspection and by the difference in redshift, clearly not part of the galaxy to which they were assigned. These 16 objects were added back into the Main Survey (`VIS_CLASS`=1).

After the redshifts were all assigned to the survey objects, we further inspected two distinct categories: very bright objects ( $r_{\text{pet}} < 17.5$  mag, 9453 objects); and targets for which no redshift was recovered (2083 objects). The original visual classification was made using the SDSS jpg image tools (Lupton et al. 2004; Neito-Santisteban, Szalay & Gray 2004). Here we also created postage stamp images

by combining the  $u, r, K$  images, and the resulting 11536 images were visually inspected by SPD. It became clear that many of the missed apparently bright galaxies were in fact probably not galaxies or at least much fainter; and some of the other apparent targets were also probably much fainter. A `VIS_CLASS` value of 4 was introduced meaning “compromised photometry (selection mag has serious error)”. From the inspection, 50 objects were classified as `VIS_CLASS`=4 and 40 objects as `VIS_CLASS`=2. Independent confirmation was made by IKB using the SDSS jpg image tools. In summary, a total of 626 potential targets identified by the automatic prescription described in Baldry et al. (2010) were expunged from the survey because of the visual classification ( $2 \leq \text{VIS\_CLASS} \leq 4$ ). These objects are identified in the `GamaTiling` catalogue available from the data release website.

The final input catalogue (`GamaTiling`) therefore constitutes 30331, 50924, and 33261 objects above the Main  $r$ -band Survey limits of  $r_{\text{pet}} < 19.4$ ,  $r_{\text{pet}} < 19.8$ , and  $r_{\text{pet}} < 19.4$  mag in G09, G12 and G15 respectively. Fig. 9 shows the normalised galaxy number-counts in these three fields indicating a significant variation between the three fields and in particular a significant underdensity in G09 to  $r_{\text{pet}} = 19.0$  mag. This will be explored further in section 4.3.

## 3 ADDITIONAL IMAGE ANALYSIS PRODUCTS

At this point we have two distinct catalogues: the input catalogue (`GamaTiling`) used by the tiling algorithm, which defines all viable target galaxies within the GAMA regions; and the combined redshift catalogue (`GamaRedshifts`), which consists of the pre-existing redshifts and those acquired by the GAMA Team and described in detail in the previous

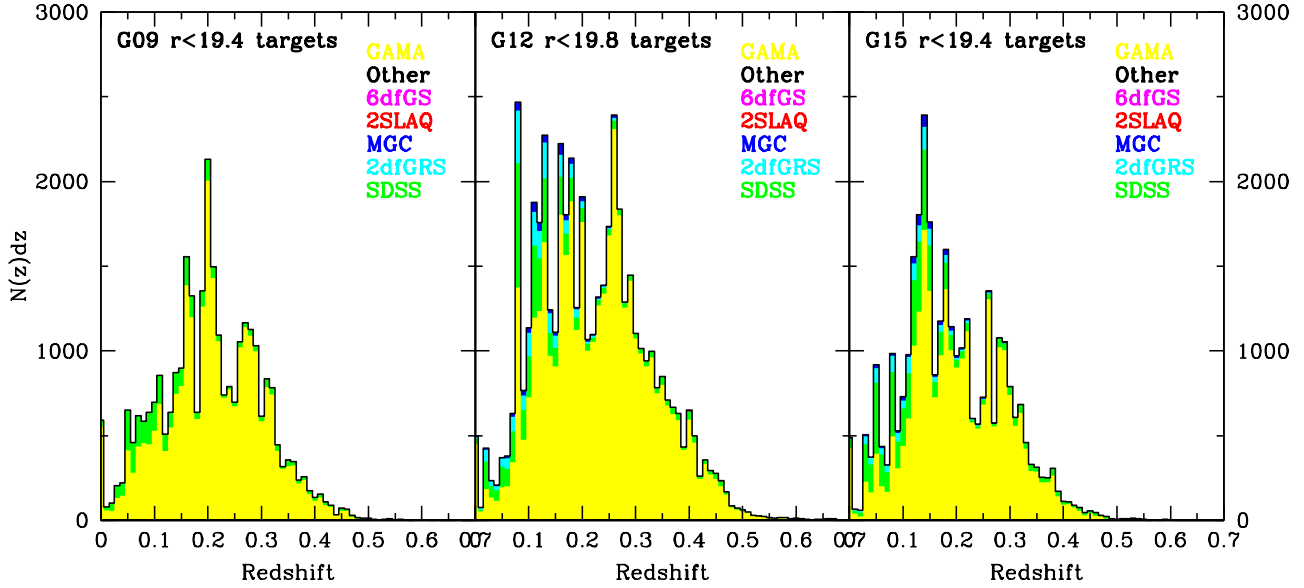


**Figure 8.** The  $n(z)$  distributions of the GAMA regions including new GAMA redshifts (shown in yellow) alongside pre-existing redshifts already in the public domain as indicated.

**Table 2.** Contribution from various surveys to the final GAMA database.

| Survey<br>source (Z_SOURCE) | G09<br>$r < 19.4$ | G12<br>$r < 19.8$ | G15<br>$r < 19.4$ | Reference or<br>Acknowledgment  |
|-----------------------------|-------------------|-------------------|-------------------|---------------------------------|
| SDSS DR7                    | 3190              | 4758              | 5092              | Abazajian et al. (2009)         |
| 2dFGRS                      | 0                 | 2107              | 1196              | Colless et al. (2001)           |
| MGC                         | 0                 | 612               | 497               | Driver et al. (2005)            |
| 2SLAQ-LRG                   | 2                 | 49                | 13                | Canon et al. (2006)             |
| GAMAZ                       | 26783             | 42210             | 25858             | This paper                      |
| 6dFGS                       | 7                 | 14                | 10                | Jones et al. (2009)             |
| UZY                         | 3                 | 2                 | 1                 | Falco et al. (1999)             |
| 2QZ                         | 0                 | 31                | 5                 | Croom et al. (2004)             |
| 2SLAQ-QSO                   | 1                 | 1                 | 1                 | Croom et al. (2009)             |
| NED                         | 0                 | 2                 | 3                 | The NASA Extragalactic Database |
| z not known                 | 347               | 1145              | 591               | —                               |
| Total                       | 30333             | 50931             | 33267             | —                               |
| Completeness (%)            | 98.9%             | 97.8%             | 98.0%             |                                 |

section. Our core catalogues consist of the combination of these two catalogues with three other catalogues containing additional measurements based on the *ugrizYJHK* imaging data from SDSS DR6 and UKIDSS LAS archives. These additional catalogues are: *GamaPhotometry*, *GamaSersic*, and *GamaPhotoz* and are briefly described in the sections below (for full details see Hill et al, 2010a; Kelvin et al. in prep. and Parkinson et al. in prep). These five catalogues are then combined and trimmed via direct name matching to produce the GAMA Core dataset (*GamaCore*), which represents the combined data from these five catalogues.

### 3.1 *ugrizYJHK* matched aperture photometry (GamaPhotometry)

A key science objective of GAMA is to provide cross-wavelength data from the far ultraviolet to radio wavelengths. The first step in this process is to bring together the available optical and near-IR data from the SDSS and UKIDSS archives. Initially the GAMA team explored simple table matching, however this highlighted a number of issues, most notably: differences in deblending outcomes, aperture sizes, and seeing between the SDSS and UKIDSS datasets. Furthermore as the UKIDSS *YJHK* data frames are obtained and processed independently in each band by The Cambridge Astronomical Survey Unit group there is the potential for inconsistent deblending outcomes, incon-

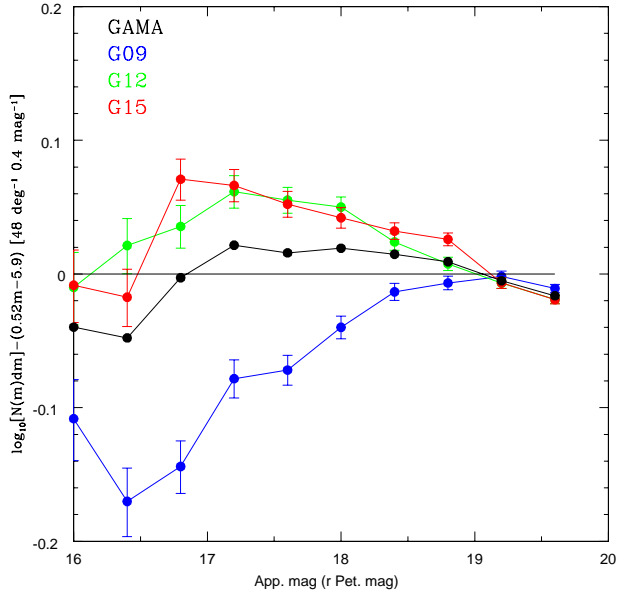


**Figure 9.** Normalised number-counts as indicated for the three regions and the average. Error bars are based on Poisson statistics suggesting an additional source of error, most likely cosmic (sample) variance between the three GAMA fields. The data becomes consistent only at  $r_{\text{pet}} > 19$  mag.

sistent aperture sizes and seeing offsets between the  $YJHK$  bandpasses. Finally both SDSS and UKIDSS LAS measure their empirical magnitudes (Petrosian and Kron) using circular apertures (see Kron 1980 and Petrosian 1976). For a partially resolved edge-on system this can result in either underestimating flux or adding unnecessary sky signal increasing the noise of the flux measurement and compounding the deblending issue. To overcome these problems the GAMA team elected to re-process all available data to provide matched aperture photometry from  $u$  to  $K$  using elliptical Kron and Petrosian apertures defined using the  $r$ -band data (our primary selection waveband). This process and comparisons to the original data are outlined in detail in Hill et al. (2010a) and described here in brief as follows:

All available data are downloaded and scaled to a uniform zeropoint in the strict AB magnitude system (i.e., after first correcting for the known SDSS to AB offset in  $u$  and  $z$  bands and converting the UKIDSS LAS from Vega to AB, see Hill et al. 2010b for conversions). Each individual data frame is convolved using a Gaussian PSF to yield consistent  $2.0''$  FWHM PSF measurements for the intermediate flux stars. The data frames (over 12,000) are then stitched into single images using the SWARP software developed by the TERAPIX group (Bertin et al. 2002) resulting in twenty-seven 20 Gb images each of  $12 \times 4 \text{ deg}^2$ . at  $0.4'' \times 0.4''$  pixel sampling. The SWARP process removes the background using the method described in SExtractor (Bertin & Arnouts 1996) using a  $256 \times 256$  pixel mesh. SExtractor is then applied to the  $r$ -band data to produce a master catalogue and rerun in each of the other 8 bandpasses in dual object mode to ensure consistent  $r$ -defined Kron apertures ( $2.5R_K$ , see Kron 1980) from  $u$  to  $K$ . As the data have been convolved to the same seeing no further correction to the colours are re-

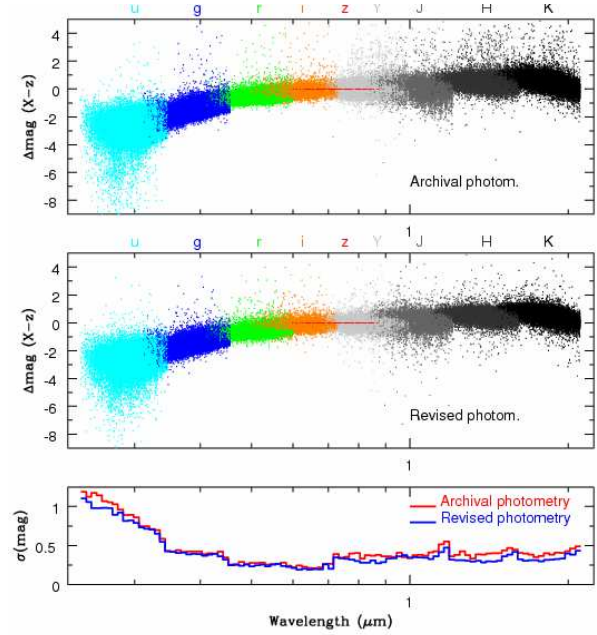


**Figure 10.** (Upper) all main survey galaxies are plotted according to their colour relative to  $J$ -band at their observed wavelength. The data points combine to make a global spectral energy distribute for the galaxy population at large. Outlier points are typically caused by an erroneous data point in any particular filter. (center) the same plot but using the revised photometry. The lower panel shows the  $5\sigma$ -clipped standard deviation for these two distributions indicating that in the  $uYJHK$  bands the colour distribution is quantifiably narrower reflecting an improvement in the photometry, providing a cleaner dataset for detailed SED modeling. Only data with photometry in all bands and with secure redshifts less than 0.5 are shown for clarity.

quired. For full details see Hill et al., (2010a). Fig. 10 shows the  $u$  to  $K$  data based on archival data (upper) and our reanalysis of the archival data (centre). The data points are plotted as a colour offset with respect to  $z$ -band at their rest wavelengths, hence the data stretch to lower wavelengths within each band with redshift. As the  $k$  and  $e$  corrections are relatively small in  $z$ -band the data dovetails quite nicely from one filter to the next. The lower panel shows the standard deviation within each log wavelength interval indicating the colour range over which the data are spread. In the  $U$  and  $YJHK$  bands the colour distribution is noticeably narrower for the revised photometry (blue line) over the archival photometry (red line). This indicates a quantifiable improvement in the photometry in these bands over the original archival data with the majority of the gain occurring for objects in more crowded regions. GamaPhotometry contains  $r$ -band detections with matched aperture photometry for  $\sim 1.9$  million objects, 1 million of which are matched to SDSS DR6 objects. The photometric pipeline is described in full in Hill et al. (2010a) and all SWARP images are made publicly available for downloading at the GAMA website.

### 3.2 Sersic profiles (GamaSersic)

By design both Petrosian and Kron magnitude systems recover only a proportion of a galaxy's flux. For the two most commonly discussed galaxy profiles, the exponential and the

de Vaucouleurs profiles, traditionally used to describe galaxy discs or spheroids, the Kron measurement recovers 96 and 90 per cent while the SDSS implementation of the Petrosian profile recovers 98 per and 83 per cent respectively (see Graham & Driver 2005). These two profiles are two specific cases of the more general Sérsic profile introduced by Sérsic (1963, 1968) and more recently reviewed by Graham & Driver (2005). The Sérsic profile (see Eqn. 1) is a useful general description of a galaxy’s overall light profile and has also been used to profile the dark matter distribution in numerical simulations (see Merritt et al. 2006):

$$I(r) = I_o \exp\left(-\left(r/\alpha\right)^{1/n}\right). \quad (1)$$

The Sérsic model has three primary parameters (see Eqn. 1), which are the central intensity ( $I_o$ ); the scale-length ( $\alpha$ ); the Sérsic index ( $n$ ); and two additional parameters for defining the ellipticity ( $\epsilon$ ) and the position angle ( $\theta$ ). Note this expression can also be recast in terms of the effective surface brightness and half-light radius (see Graham & Driver 2005 for a full description of the Sérsic profile). The Sérsic index might typically range from  $n = 0.5$  for diffuse systems to  $n = 15$  for concentrated systems. If a galaxy’s Sérsic profile is known it is possible to integrate this profile to obtain a total magnitude measurement, and this mechanism was used by the SDSS to provide model magnitudes by force fitting either an  $n = 1$  (exponential) or an  $n = 4$  (de Vaucouleurs) profile to all objects. Here we attempt to take the next step, which is to derive the Sérsic profile with  $n$  as a free parameter, in order to provide total magnitudes for all targets.

As described in full in Kelvin et al. (2010, in prep.) we use the GALFIT3 package (Peng et al. 2010) to fit all galaxies to SDSS DR6  $r_{\text{pet}} < 22.0$  mag. In brief the process involves the construction of comparable SWARP’ed images as in section 3.1 but without Gaussian PSF convolution (raw SWARPS). Instead, the PSF at the location of every galaxy is derived using 20 intermediate brightness stars from around the galaxy as identified by SExtractor and modeled by the code PSFex (Bertin priv. comm.). Using the model PSF the 2D Sérsic profile is then derived via GALFIT3, which convolves a theoretical profile with the PSF and minimises the five free parameters. The output Sérsic total magnitude is an integral to infinite radius, which is unrealistic. However relatively little is known as to how the light profile of galaxies truncate at very faint isophotes with all variants seen (Pohlen & Trujillo 2006).

In order to calculate an appropriate Sérsic magnitude it is prudent to adopt a truncation radius out to which the Sérsic profile is integrated. For SDSS model magnitudes exponential ( $n = 1$ ) profiles were smoothly truncated beyond  $3R_e$  and smoothly truncated beyond  $7R_e$  for de Vaucouleurs ( $n = 4$ ) profiles. Here we adopt an abrupt truncation radius of  $10R_e$ ; for the majority of our data, this equates to an isophotal detection limit in the  $r$ -band of  $\sim 30$  mag/sq arcsec — the limit to which galaxy profiles have been explored. We note for almost all plausible values of  $n$ , the choice of a truncation radius of  $7R_e$  or  $10R_e$  introduces a systematic uncertainty that is comparable or less than the photometric error. Fig. 11 shows a comparison of the three principle photometric methods, with  $r_{\text{pet}} - r_{\text{Kron}}$  versus  $\log_{10}(n)$  (upper),  $r_{\text{pet}} - r_{\text{Sersic}10R_e}$  versus  $\log_{10}(n)$  (middle), and  $r_{\text{Kron}} - r_{\text{Sersic}10R_e}$  versus  $\log_{10}(n)$  (lower). Note that it

is more logical to compare to  $\log_{10}(n)$  than  $n$  as it appears in the exponent of the Sérsic profile definition (see review of the Sérsic profile in Graham & Driver 2005 for more information). The top panel indicates that our Kron photometry (defined in section 3.1), reproduces (with scatter) the original SDSS photometry. As described in the previous section the motivation for rederiving the photometry is to provide elliptical matched apertures in *ugrizYJHK*. The middle and lower plots shows a significant bias between these traditional methods (Petrosian and Kron) and the new Sérsic10  $R_e$  magnitude. The vertical lines indicate the location of the canonical exponential and de Vaucouleurs profiles. For normal discs and low- $n$  systems the difference is negligible. However for  $n > 4$  systems the difference becomes significant. This is particularly crucial as the high- $n$  systems are typically the most luminous and most massive galaxy systems (Driver et al. 2006). Hence a bias against this population can lead to serious underestimation of the integrated properties of galaxies, e.g., integrated stellar mass or luminosity density (see Fig. 21 of Hill et al. 2010a, where a 20 per cent increase in the luminosity density is seen when moving from Petrosian to Sérsic magnitudes). The Sérsic  $10R_e$  magnitudes are therefore doing precisely what is expected, which is to recover the flux lost via the Petrosian or Kron photometric systems.

GamaSersic contains the five parameter Sérsic output for all 1.2 million objects with SDSS DR6  $r_{\text{pet}} < 22$  and full details of the process are described in Kelvin et al. (in prep.). At the present time we only include in our core catalogues the individual profiles for each object and the `r_SERS_MAG_10RE` -parameter (see Table A2) while final checks are being conducted. We release the total correction to allow for an early indication of the Kron-Total mag offset but caution that these values may change. Similarly we include for individual objects all profiles with the full Sérsic information specified but again caution that these may change slightly over the next few months as further checks continue. If colour gradients are small then the  $r$ -band Kron to Total magnitude offset given by `r_SERS_MAG_10RE` can be applied to all filters.

### 3.3 Photometric redshifts (GamaPhotoz)

The GAMA spectroscopic survey is an ideal input dataset for creating a robust photometric redshift code that can then be applied across the full SDSS survey region. Unlike most spectroscopic surveys, GAMA samples the entire SDSS  $r$ -band selected galaxy population in an extensive and unbiased fashion to  $r_{\text{pet}} = 19.8$  mag — although for delivery of robust photo- $z$ ’s to the full depth of SDSS, it is necessary to supplement GAMA with deeper data. Below we briefly summarize the method, explained in greater detail in Parkinson et al. (in prep.).

We use the Artificial Neural Network code ANNz (Collister & Lahav 2004) with a network architecture of N:2N:2N:1, where N=6 is the number of inputs to the network (5 photometric bands and one radius together with their errors). In order to develop a photo- $z$  code valid for the full-SDSS region we use the *ugriz* übercalibration of SDSS DR7 (Padmanabhan al. 2008), together with the best of the De Vaucouleurs or Exponential half-light radius measurement for each object (Abazajian et al. 2009). Our

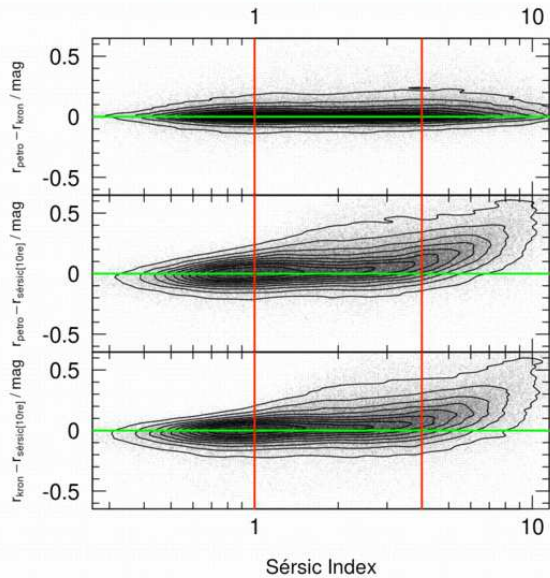


**Figure 11.** Original SDSS Petrosian magnitudes versus our SExtractor based Kron magnitudes (top), original SDSS Petrosian magnitudes versus our GALFIT3 Sérsic magnitudes (integrated to  $10R_e$ ) (middle), and our SExtractor Kron versus our GALFIT3 Sérsic magnitudes (integrated to  $10R_e$ ) (lower). Contours vary from 10 per cent to 90 per cent in 10 per cent intervals.

training set is composed of all GAMA spectroscopic redshifts and zCOSMOS spectroscopic redshift (Lilly et al. 2007), as well as the 30-band COSMOS photometric redshifts (Ilbert et al. 2009). With a redshift error of  $< 0.001$ , these are as good as spectroscopy when it comes to calibrating 5-band photo- $z$ 's from SDSS alone. The corresponding fractions in the training, validating and testing sets are 81 per cent, 4 per cent and 15 per cent respectively, with over 120k galaxies in total. For COSMOS (and hence zCOSMOS) galaxies, we perform a careful matching to SDSS DR7 objects. This large, complete, and representative photo- $z$  training set allows us to use an empirical regression method to estimate the errors on individual photometric redshifts. The left panel of Fig. 12 shows that up to  $z_{\text{ph}} \approx 0.40$  the bias in the median recovered photo- $z$  is less than  $0.005/(1 + z_{\text{ph}})$ , while beyond it (not shown) the bias is typically within  $0.01/(1 + z_{\text{ph}})$ . Considering the random errors on the individual estimates, this systematic bias is negligible, while still very well quantified. The right panel of Fig. 12 presents the equivalent plot using SDSS DR7 photometric redshifts, as listed in the Photoz table of the SDSS Sky Server. In both cases, these plots show only galaxies with  $r_{\text{pet}} < 19.8$  mag. This comparison

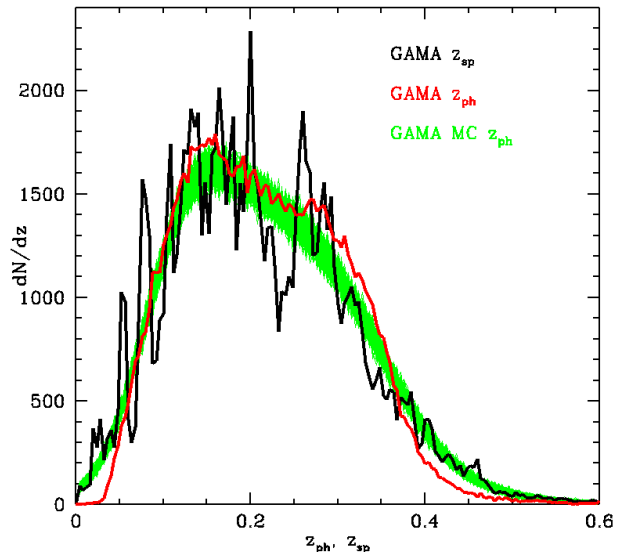


**Figure 13.** Spectroscopic redshift distribution of GAMA galaxies (black), the corresponding photo- $z$  distribution of GAMA galaxies (red) and one thousand Monte-Carlo generated photo- $z$  distributions, including the Gaussianly distributed photo- $z$  error (green).

highlights the importance of using a complete and fully representative sample in the training of photometric redshifts.

For an extensive and complete training set such as GAMA, it is possible to derive a simple and direct method for calculating photo- $z$  errors. We estimate the photo- $z$  accuracy in a rest-frame colour magnitude plane with several hundreds of objects per  $0.1 \times 0.1$  mag bin down to  $r_{\text{pet}} = 19.8$  mag, and typically about fifty objects per  $0.1 \times 0.1$  mag bin down to  $r_{\text{pet}} \approx 21.5$  mag. This method provides a robust normally distributed error for each individual object. We note that with this realistic photo- $z$  error it is possible to correctly recover the underlying spectroscopic redshift distribution with our ANNz photometric redshifts as illustrated in Fig. 13. It is interesting to note that, without this added error, the raw photo- $z$  histogram is actually narrower than the spectroscopic histogram. This makes sense, because photo- $z$  calibration yields no bias in true  $z$  at given  $z_{\text{phot}}$ : it is thus inevitable that there is a bias in  $z_{\text{phot}}$  at given true  $z$ , which is strong wherever  $N(z)$  changes rapidly; this effect can be seen in operation in the ranges  $z < 0.05$  and  $0.3 < z < 0.5$ . GamaPhotoz contains both photometric redshifts and errors for all systems to  $r_{\text{model}} < 21.5$  mag and the code is currently being applied across the full SDSS region. We plan to release our prescription for these improved all-SDSS photo- $z$ 's by the end of 2010. In the meantime, we are open to collaborative use of the data: contact [gama@gama-survey.org](mailto:gama@gama-survey.org).

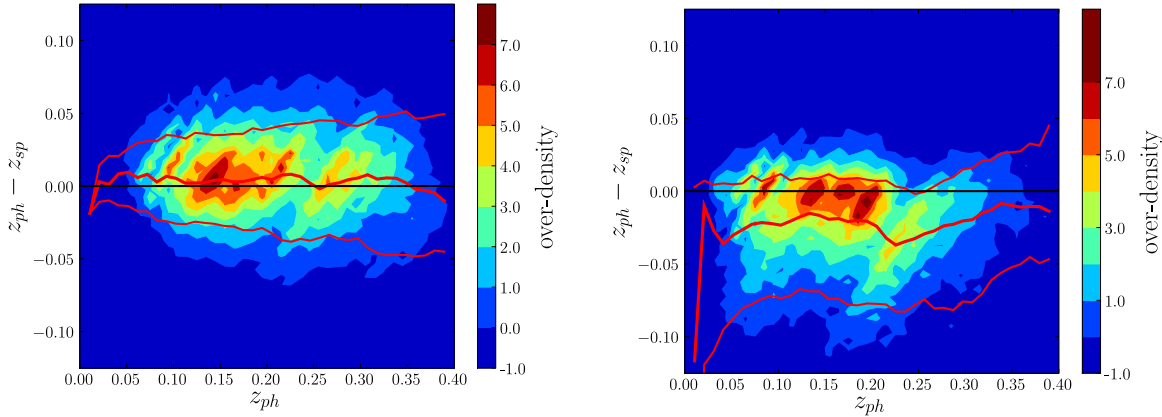


**Figure 12.** (left) GAMA photometric and spectroscopic redshift comparison as a function of the photometric redshift for GAMA galaxies, colour coded as function of galaxy (over-)density. The thick red central line shows the median, while the outer lines delineate the central 68 per cent of the distribution as function of  $z_{ph}$ . (right) Same as the left panel, but for the SDSS photometric redshift estimate, extracted from the Photoz table in SDSS DR7.

#### 4 BUILDING AND TESTING THE GAMA CORE CATALOGUES

We can now combine the five catalogues described above to produce the *GamaCore* catalogue of  $\sim 1$  million objects, which contains what we define as our core product to  $r < 22$  mag. Figs 14–16 uses this catalogue to illustrate the progression of the redshift survey over the years through the build-up of the cone plots in the three distinct regions. As the survey has progressed the fidelity with which structure can be resolved and groups identified has increased significantly. In the final maps the survey is over 98% complete with a near uniform spatial completeness for all three regions thanks to the “greedy” targeting algorithm (see Robotham et al., 2010). From *GamaCore* we now extract three science ready subsets:

(1) GAMA data release 1 (*GamaCoreDR1*), which includes the majority of spectroscopic data acquired in year 1 with  $r_{\text{pet}} < 19.0$  mag and a central strip in G12 ( $\delta \pm 0.5^\circ$ ) to  $r_{\text{pet}} < 19.8$  mag and which forms our primary public data release product at this time.

(2) GAMA Science (*GamaCoreMainSurvey*), which includes all objects within our main selection limits and suitable for scientific exploitation by the GAMA team and collaborators.

(3) GAMA-Atlas (*GamaCoreAtlasSV*), which includes all year 1 and year 2 data with reliable matches to the H-ATLAS science demonstration catalogue as described in Smith et al. (2010) and is currently being used for science exploitation by the H-ATLAS team. For further details and for the H-ATLAS data release see <http://www.h-atlas.org>

In the following section we explore the properties of the two primary catalogues (*GamaCoreDR1* and *GamaCoreMainSurvey*) and do not discuss *GamaAtlasSV* any further.

##### 4.1 Survey completeness

In Fig. 6 we showed the completeness of the GAMA redshift survey only. This was given by the number of objects with secure redshifts divided by those targeted during the

three year spectroscopic campaign. In Fig. 17 we show the equivalent completeness but now for the combined data as described in section 2.8 for our two principle scientific catalogues (*GamaCoreDR1* and *GamaCoreMainSurvey*). This is given by the known redshifts in the GAMA regions divided by the known targets in the GAMA region. The blue regions show the pre-existing redshifts acquired before GAMA commenced and is mainly dominated by the SDSS DR6 with a spectroscopic limit of  $r_{\text{pet}} < 17.77$  mag (cf. Table 2). *GamaCoreDR1* is shown in green where the main focus in year 1 was to survey objects brighter than  $r_{\text{pet}} = 19$  mag with the exception of a central strip in the G12 region (motivated by the desire to assess the completeness function in preparation for year 2 and 3 observations).

*GamaCoreDR1* is relatively complete to  $r_{\text{pet}} < 19.0$  mag and the residual spatial bias can be compensated for by using the survey masks provided (see section 5). After year 3 observations (*GamaCoreMainSurvey*) one can see 95 per cent or greater completeness in all apparent magnitude intervals with a smooth tapering off from 99 to 95 per cent completeness in the faintest 0.5mag interval. As all targets without a redshift have now been visually inspected this fall in completeness is real and obviously needs to be taken into consideration in any subsequent analysis. However GAMA remains the most complete survey published to date with the 2dFGRS achieving a mean survey completeness of 90 per cent to  $b_J = 19.45$  mag, SDSS 90 per cent to  $r_{\text{pet}} = 17.77$  mag, and the MGC 96 per cent to  $B = 20$  mag.

##### 4.2 Survey bias checks

In Fig. 17 we see a small but non-negligible completeness bias with apparent magnitude, hence it is worth checking for any bias in the obvious parameter space of colour, surface brightness, concentration, and close pairs. We explore the first three of these in Fig. 18 for year 1 data (left), year 2 data (centre) and year 3 data (right). The colour indicates the degree of completeness in these two-dimensional planes and the contours show the location of the bulk of the galaxy population. In all three cases there is no strong hori-

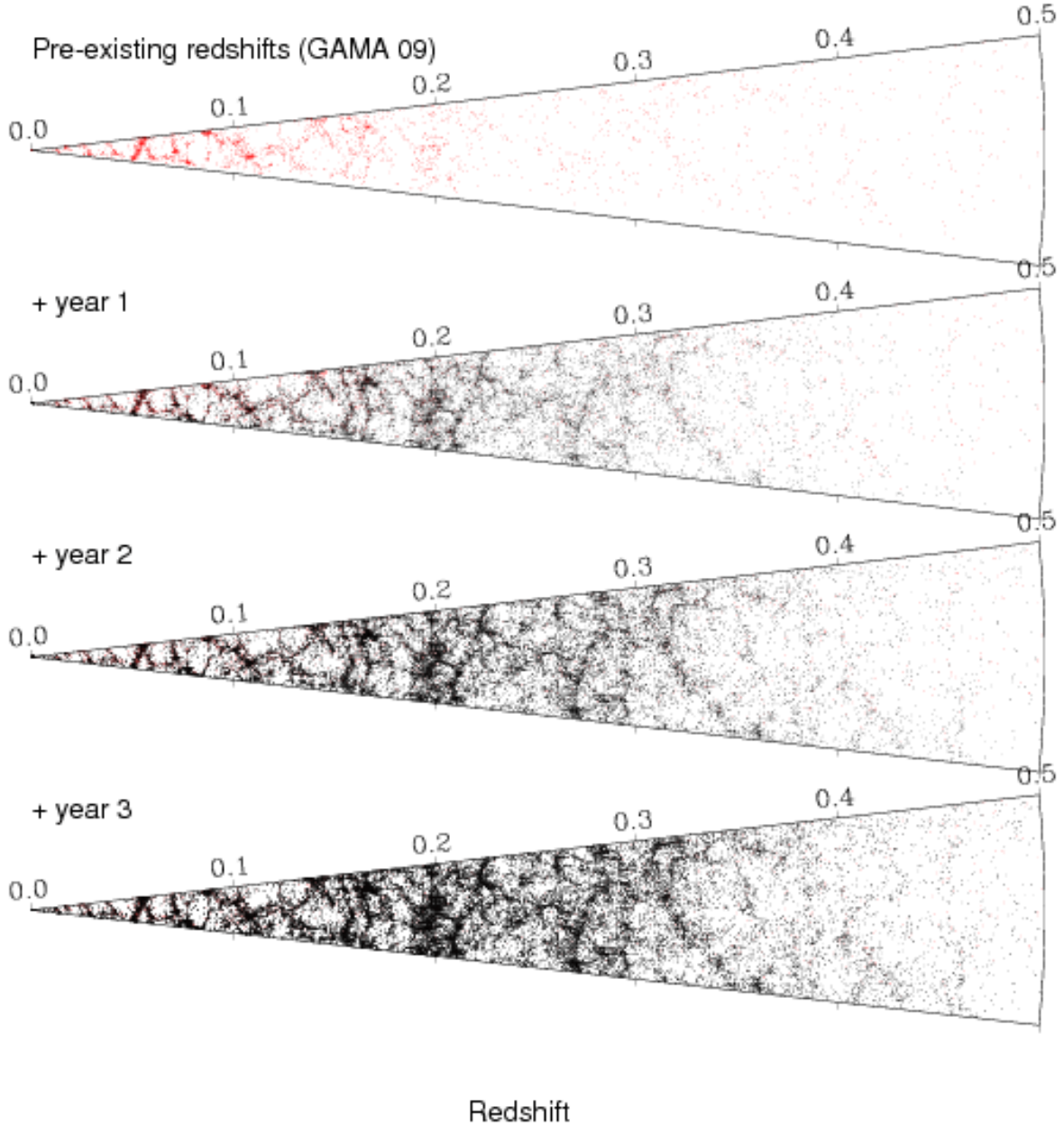


**Figure 14.** Redshift cone diagram for the GAMA 09 region showing (top to bottom), pre-existing data, year 1 data release added, year 2 data release added, year 3 data release added.

zontal bias that would indicate incompleteness with colour, surface brightness, or concentration. This is not particularly surprising given the high overall completeness of the survey, which leaves little room for bias in the spectroscopic survey, but we acknowledge the caveat that bias in the input catalogue cannot be assessed without deeper imaging data. Note that in these plots surface brightness is defined by:  $\mu_{\text{eff}} = r_{\text{pet}} + 2.5 \log_{10}(2\pi ab)$  where  $a$  and  $b$  are the major and minor half-light radii as derived by GALFIT3 (see Kelvin et al. 2010 in prep, for details of the fitting process)

and concentration is defined by  $\log_{10}(n)$  where  $n$  is the Sérsic index derived in section 3.2.

A major science priority of the GAMA programme is to explore close pairs and galaxy asymmetry (e.g., De Propris et al. 2007). As GAMA is a multi-pass survey with each region of sky being included in 4-6 tiles (see Fig. 2), the close pair biases due to minimum fibre separations, which plague the 2dFGRS, SDSS, and MGC studies, are overcome. Fig. 19 shows the redshift completeness versus neighbour class. The neighbour class of any galaxy is defined (see Baldry et al. 2010) as the number of target galaxies within a



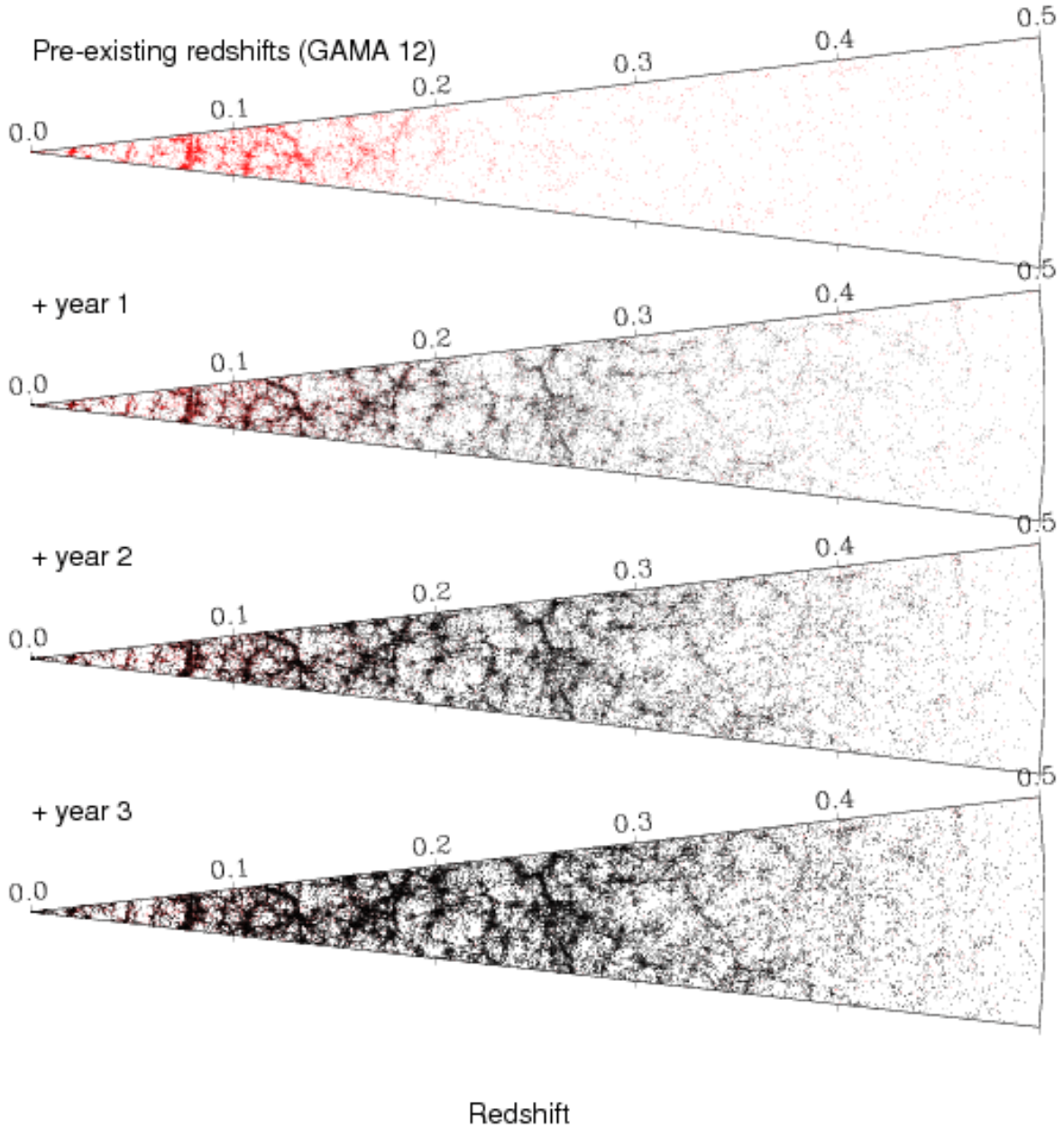


**Figure 15.** Redshift cone diagram for the GAMA 12 region showing (top to bottom), pre-existing data, year 1 data release added, year 2 data release added, year 3 data release added.

40'' radius. The nominal 2dF fibre-collision radius. The figures shows the progress towards resolving these complexes at the outset and after each year the survey has been operating. All low neighbour class objects are complete with only a few redshifts outstanding in a small fraction of the higher neighbour class complexes. The data therefore represents an excellent starting point for determining merger rates via close pair analyses.

### 4.3 Overdensity/underdensity of the GAMA regions

All galaxy surveys inevitably suffer from cosmic variance, more correctly stated as sample variance. Even the final SDSS, the largest redshift survey to date, suffers an estimated residual 5 per cent cosmic variance to  $z < 0.1$  (see Driver & Robotham 2010) — mainly attributable to the “Great Wall” (see Baugh et al. 2004; Nichol et al. 2006). As the GAMA regions lie fully within the SDSS it is possible to determine whether the GAMA regions are overdense or underdense as compared to the full SDSS over the un-

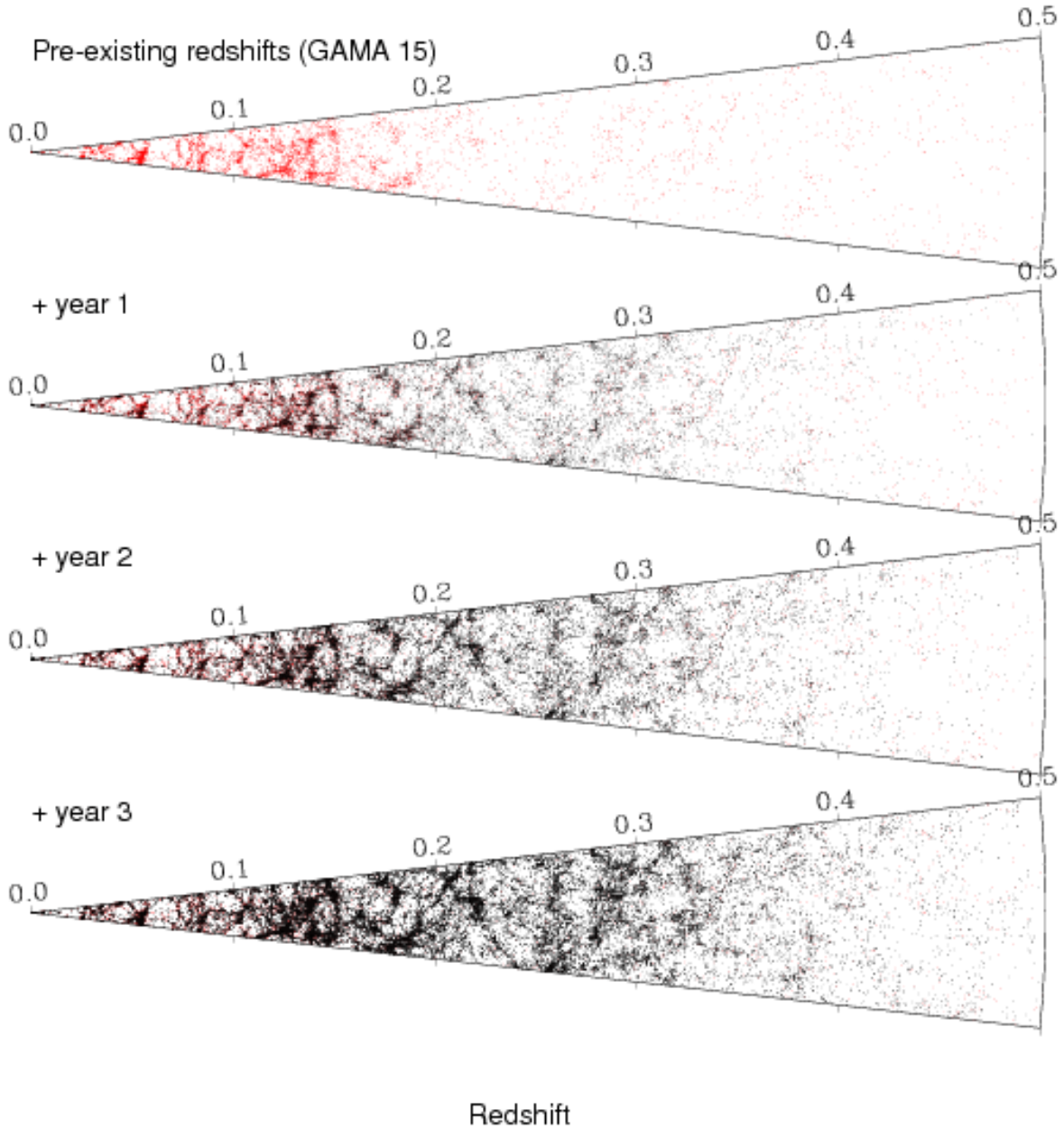


**Figure 16.** Redshift cone diagram for the GAMA 15 region showing (top to bottom), pre-existing data, year 1 data release added, year 2 data release added, year 3 data release added.

biased redshift range in common ( $z < 0.1$ ) and relative to each other at higher redshifts where the SDSS density drops due to incompleteness imposed by the  $r_{\text{pet}} < 17.77$  mag spectroscopic limit. Fig. 20 shows results with the upper panel showing the density of  $M^* \pm 1.0$  galaxies (defined as  $M^* - 5 \log h = -20.81$  mag) in 0.01 redshift intervals, for a 5000 sq.deg. region of the SDSS DR7 (blue), and for the three GAMA blocks (as indicated) and the sum of the three regions (solid black histogram). The  $k$  and  $e$  corrections adopted and the methodology, including the SDSS sample construction, are described in Driver & Robotham (2010)

but are not particularly important as we are not exploring trends with  $z$  but rather the variance at fixed  $z$ . The error bars shown are purely Poisson and so discrepancies larger than the error bars are indicative of cosmic variance induced by significant clustering along the line-of-sight. The middle and lower panels show the sum of these density fluctuations relative to either SDSS (middle) or the average of the three GAMA fields (lower). Note that these panels (middle, lower) now show the density fluctuation *out to* the specified redshift as opposed to *at* a specific redshift (top), i.e., the cosmic variance. We can see that out to  $z = 0.1$  the three GAMA fields

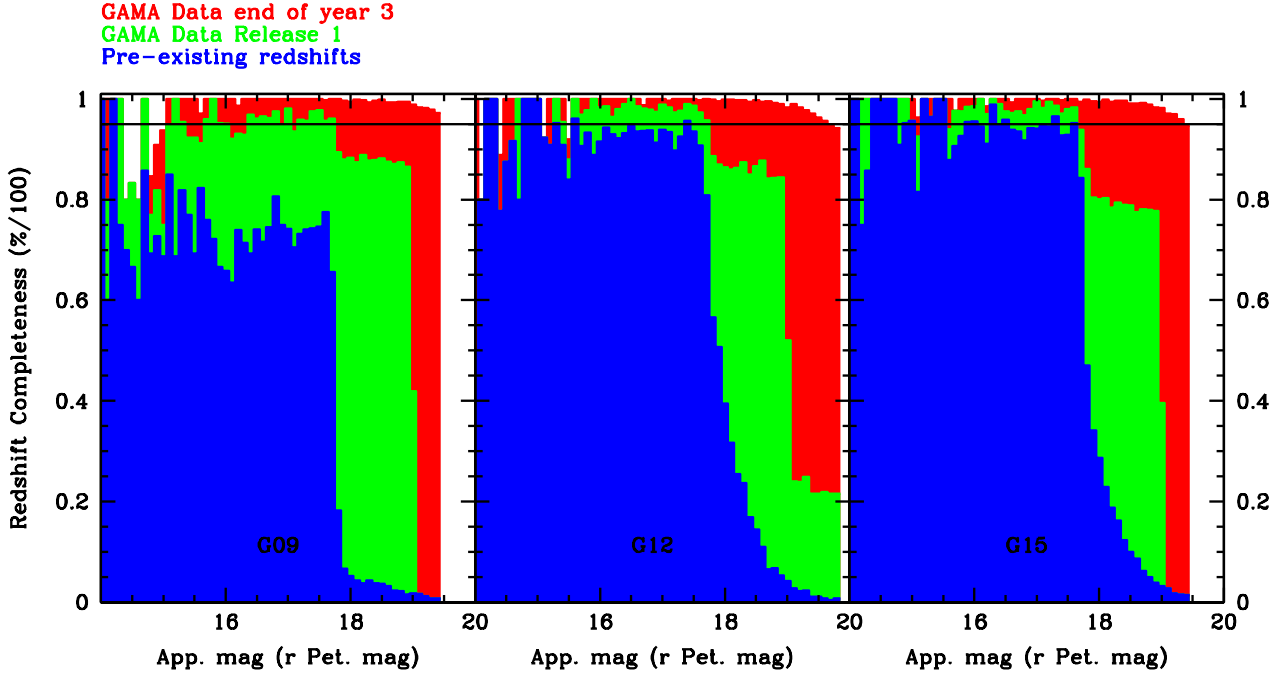


**Figure 17.** The final completeness of the combined redshift catalogues prior to survey commencing (blue), after GamaCoreDR1 (green) and GamaCoreMainSurvey (red) for G09, G12 and G15 (left to right). In all cases the solid black lines shows 95 per cent completeness.

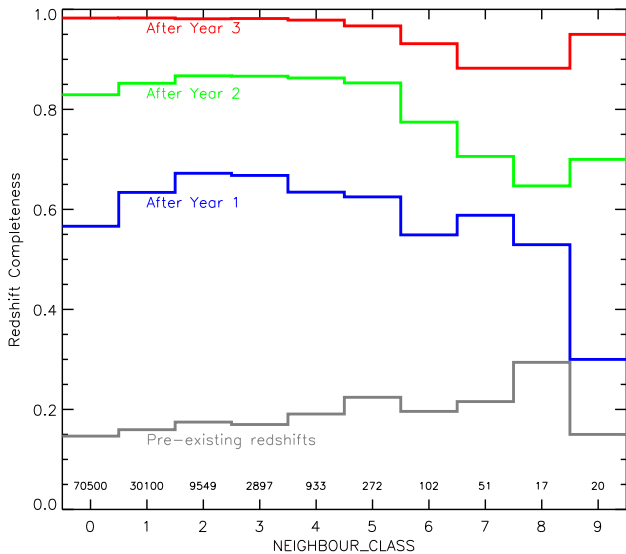


**Figure 19.** The redshift completeness as a function of Neighbour Class (NC). NC is defined for each target as the number of other Main Survey targets within  $40''$  (numbers with each NC value are annotated in the figure). The various lines show the progress in resolving clustered objects at the outset and after each year of observations for the  $r$ -limited Main Survey. Note the bias toward  $NC > 0$  after Year 1 and 2 is the result of increasing the priority of clustered targets (Robotham et al. 2010) in order to avoid being biased against  $NC > 0$  after Year 3. The final survey has fully resolved almost all close complexes leaving only a minimal bias when determining merger rates via close pairs: the redshift completeness is  $> 95\%$  for  $NC \leq 5$ .

are overall 15 per cent under dense with respect to a 5000 sq.deg. region of SDSS DR7 (NB: the volume surveyed by the SDSS comparison region is  $\sim 1.3 \times 10^7 h^{-3} \text{Mpc}^3$ ). This is extremely close to the 15 per cent predicted from Table 2 of Driver & Robotham (2010). Beyond  $z = 0.1$  one can only compare internally between the three GAMA fields. The inference from Fig. 20 is that for any study at  $z < 0.2$  the cosmic variance between the three regions is significant with G09 in particular being under-dense for all redshifts  $z < 0.2$  when compared to the other two regions (NB: the volume surveyed within the combined GAMA regions to  $z < 0.2$  is  $\sim 2.8 \times 10^6 h^{-3} \text{Mpc}^3$ ). It is therefore important when considering any density measurement from GAMA data to include the cosmic variance errors indicated in Fig. 20. For example a luminosity function measured from the G09 region only out to  $z = 0.1$  would need to be scaled up by  $\times 1.41$  etc.

## 5 MASKS

For accurate statistical analysis of GAMA it is essential to have a full understanding of the criteria that define its parent photometric catalogue, and also of the spatial and magnitude-dependent completeness of the redshift catalogue. For this purpose we have defined three functions characterizing this information as a function of position on the sky and magnitude selection. Here we present briefly the two most important ones, i.e. the survey imaging mask function and the redshift completeness mask relative to the main  $r_{\text{pet}}$  survey limits. The combination of both functions is key for any spatially dependent measurements based on GAMA data, and in particular on GAMA year 1 data. Additional

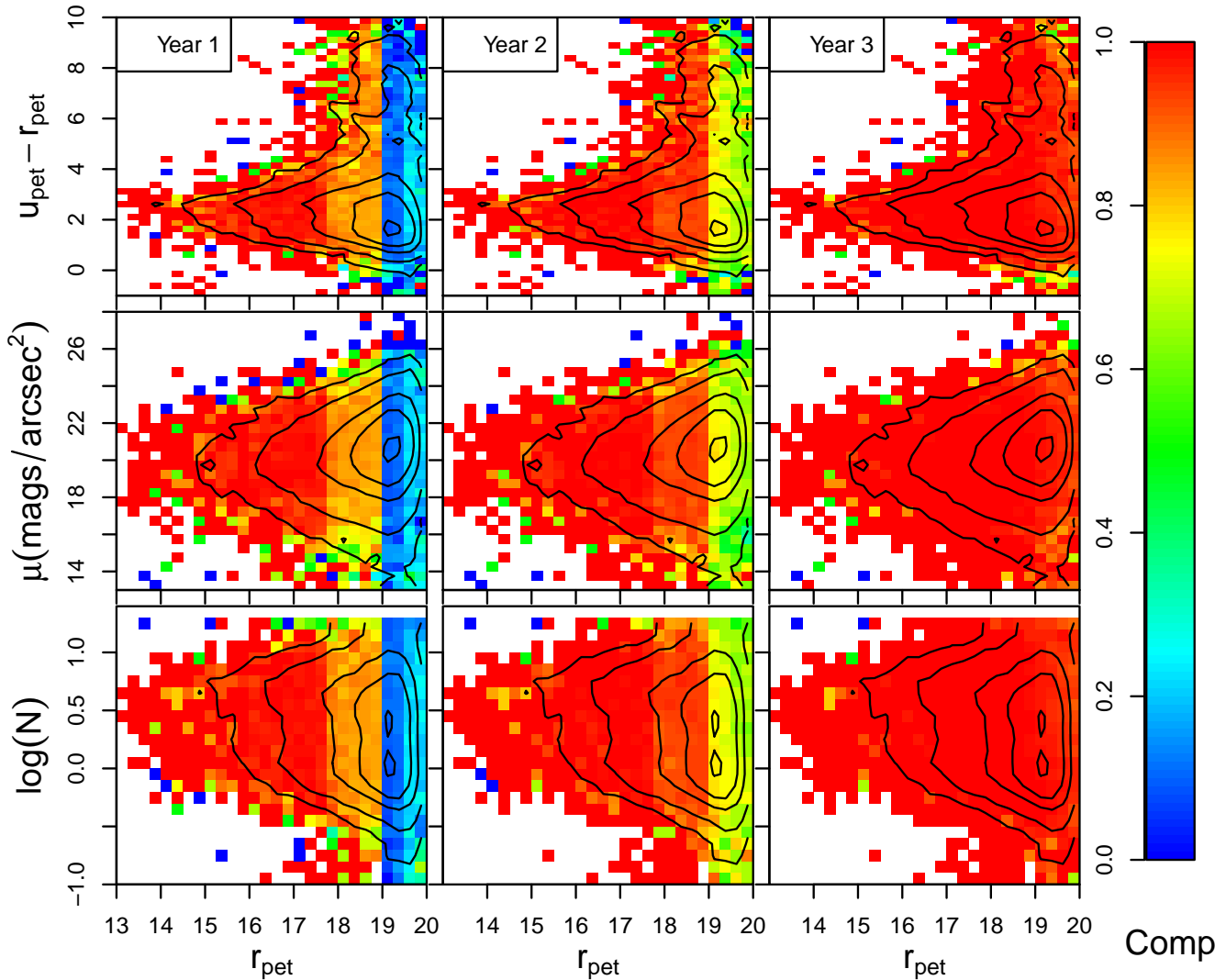


**Figure 18.** Completeness is the bivariate planes of apparent magnitude and  $u - r$  colour (top), apparent magnitude and effective surface brightness (middle), apparent magnitude and Sérsic index (bottom) for GAMA data after year 1 (left), year 2 (centre) and year 3 (right). Contours show the percentage of galaxies enclosed from out to in 99, 95, 75, 50 & 5 per cent. Apart from the progression in apparent magnitude over the three years no other obvious bias is evident.

survey completeness masks for other selections (e.g.,  $z$ ,  $K$ ) or any combination of are available to the Team and will be released shortly.

### 5.1 The imaging mask

We are interested in knowing which regions of the GAMA areas have not been properly covered by the SDSS imaging survey, or which should be excluded owing to the presence of bright stars. For that reason, we want to map out SDSS imaging areas containing any of the following information: bleeding pixel, bright star, satellite trail or hole.

First we create, following the imaging mask information available on the SDSS DR6 website<sup>3</sup>, the associated convex

polygons, delimiting areas for which imaging information is either not available or could be corrupted (as in the case of bleeding pixels). We primarily use the  $r$ -band imaging mask information, as GAMA is nominally an  $r$ -band selected survey, but for completeness we construct all five SDSS imaging masks for the GAMA areas.

Then we build an additional bright star mask based on stars down to  $V < 12$  in the Tycho 2, Tycho 1 and Hipparcos catalogues. For each star we define an exclusion radius  $r$ , defined as:

$$r = R_s/0.8 \quad \text{for } 10 < V \leq 12 \quad (2)$$

$$r = R_s/0.5 \quad \text{for } V \leq 10 \quad (3)$$

where  $R_s$  is the scattered-light radius, as estimated based on the circular region over which the star flux per pixel is greater than five times the sky noise level. Further details

<sup>3</sup> [http://www.sdss.org/dr6/products/images/use\\_masks.html](http://www.sdss.org/dr6/products/images/use_masks.html) and <http://www.sdss.org/dr6/algorithms/masks.html>

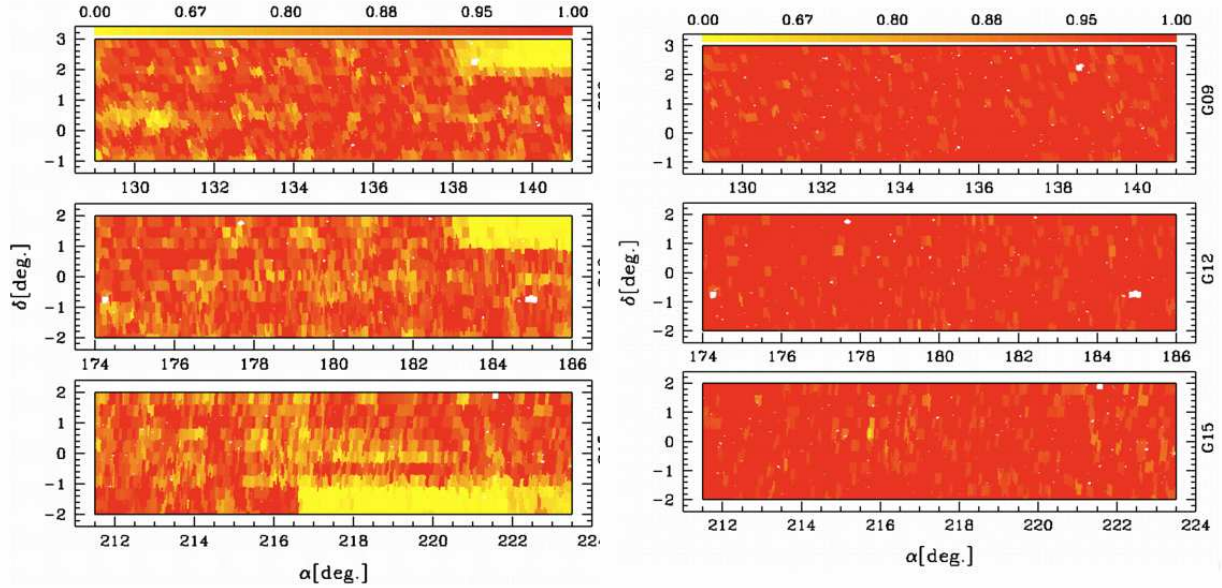


**Figure 21.** Spatial completeness masks to  $r_{\text{pet}} < 19.0$  mag after year 1 (left) and year 3 (right). The three GAMA regions are shown from top to bottom as G09, G12 and G15. The white regions indicate areas not sample either due to missing input catalogue data or bright stars.

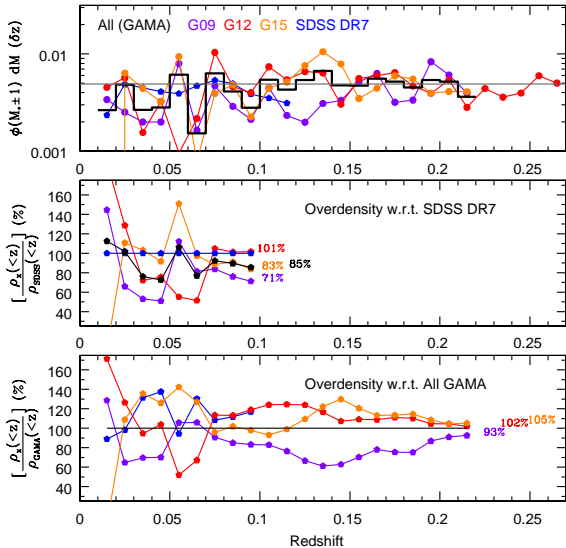


**Figure 20.** (upper) The differential number-density of  $M_* \pm 1.0$  mag galaxies in redshift intervals of 0.01. (middle) the overdensity of  $M_* \pm 1.0$  mag galaxies out to the specified redshift for the survey indicated by line colour relative to that seen in a 5000 sq.deg. region of SDSS DR7. (lower) the overdensity of  $M_* \pm 1.0$  mag galaxies out to the specified redshift for the survey indicated relative to that seen over all three GAMA regions.

on the bright star exclusion mask are given in section 3.3 of Baldry et al. (2010).

The final imaging mask function is then the union of the two separate functions. For ease of use, the imaging masks have been pixelated using an equal area projection.

## 5.2 The $r_{\text{pet}}$ redshift completeness mask

Normally a simple way to define a redshift success rate would be to make use of the geometry defined by the complete set of  $2^\circ$  fields that were used to tile the survey region for spectroscopic observations. However, due to the tiling strategy adopted in the first year, due to the preselection of observing the brightest targets first, and due to the much higher number density of galaxies than can be accommodated in a single 2dF field, this simple and straightforward approach does not account well enough for the spatial incompleteness of the survey. Therefore for year 1 data, we had to develop different completeness masks each defined for a different magnitude limit interval:

- For G09 and G15, there are two completeness masks each: one for galaxies brighter than  $r_{\text{pet}} = 19.0$  and one for  $19.0 \leq r_{\text{pet}} < 19.4$ .
- For G12, there are three completeness masks: the same two as for G09 and G15, as well as one for  $19.4 \leq r_{\text{pet}} < 19.8$ .

Once the samples for which completeness masks are needed have been defined, one just needs to provide a reasonable definition for the redshift success rate. We choose to tessellate the GAMA regions with a large number of sectors. We incorporate the relevant imaging mask at this stage, by imposing that sectors do not cover any regions masked by the imaging mask. Each sector contains between 15 and 50 galaxy targets, is limited in extent (less than 24 arcmin) and in size (less than 225 arcmin<sup>2</sup>). These conditions are necessary to avoid shot-noise dominated masks, and to guarantee that small scale information is preserved as much as possible. We note that in the current implementation these

sectors are not uniquely defined,<sup>4</sup> but once specified any given position on the sky belongs to a unique sector. For each sector,  $\theta$ , we define the redshift success rate,  $R_z(\theta)$ , for a sample of galaxies within specified magnitude limits, as the ratio of the number of galaxies for which good quality redshifts have been obtained,  $N_z(\theta)$ , to the total number of objects contained in the tiling catalogue,  $N_t(\theta)$ . The redshift completeness of a given sector,  $R_z(\theta)$ , should be clearly distinguished from the redshift completeness of a given 2dF field,  $c_F$ , since multiple overlapping fields can contribute to a single sector and  $c_F$  is a measure of the quality of the observing conditions for galaxies observed at the same time.

We present in Fig. 21 the completeness masks for all three regions for GamaCoreDR1 (left) and GamaCoreMainSurvey (right) to  $r_{\text{pet}} < 19.0$ . Completeness masks for all regions and different selections are available to the team members and collaborators only at this stage.

## 6 GAMA SCIENCE READY CATALOGUES AND DATA RELEASE 1

The combination of our five input catalogues, as outlined in section 4, constitutes our core GAMA catalogue of  $\sim 1$  million galaxies lying within the GAMA regions and extending to approximately  $r_{\text{pet}} < 22.0$  mag. This catalogue has inhomogeneous selection, is liable to be incomplete towards the faint-end, along with significant noise in the photometry at the very faint limit and spurious detections. We therefore extract from this dataset three science-ready catalogues and one overflow catalogue. These four catalogues along with the complete SWARP'ed mosaics of the GAMA regions, associated spectra bundles, images, Sérsic profiles and a variety of data inspection tools (including a MySQL access point) constitute our first data release and are now available via: <http://www.gama-survey.org/>

### 6.1 GamaCoreMainSurvey - Available 01/07/12

The GamaCoreMainSurvey is the GAMA team's principal science catalogue and is constructed from GamaCore by removing all objects outside our Main Survey limits as defined in Baldry et al. (2010). These limits are:  $r_{\text{pet}} < 19.4$  mag in G09 & G15 and  $r_{\text{pet}} < 19.8$  mag in G12 (114441 objects).  $K_{\text{Kron}} < 17.6$  with  $r_{\text{model}} < 20.5$  mag (61393 objects) or  $z_{\text{Model}} < 18.2$  with  $r_{\text{model}} < 20.5$  mag (55534 objects) and are selected using  $\text{SURVEY\_CLASS} > 3$ . For a description of the  $\text{SURVEY\_CLASS}$  parameter see Table 3). This amounts to 119 778 objects in total of which 101 576 are new redshifts provided by GAMA and 18202 pre-existing. Fig. 17 shows the completeness in the  $r$ -band however similar plots can trivially be constructed in  $z$  or  $K$ . The spectroscopic completeness (which includes objects not targeted) is 98.2 per cent in  $r$ , 99.3 per cent in  $z$  and 98.6 per cent in  $K$ . The parameters contained in this catalogue are listed in Table A2. As this is our main science catalogue we place an embargo on its public release until 1<sup>st</sup> July 2012 but are open to requests for collaboration sent to: [gama@gama-survey.org](mailto:gama@gama-survey.org)

<sup>4</sup> This could be achieved by making each target galaxy the centre of a subsector and then increasing the radius of all subsectors and create sectors by the merger of overlapping subsectors.

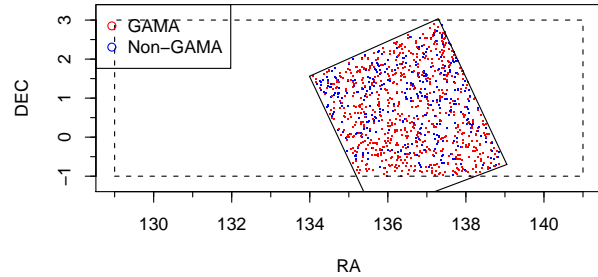


**Figure 22.** The location of the H-ATLAS SV region overlaid on the GAMA 9hr region (dotted lines) and showing the location of pre-existing (blue) and new GAMA (red) redshifts within the common region.

### 6.2 GamaCoreDR1 — Available 2010-06-25

The GamaCoreDR1 is the current GAMA Data Release 1 catalogue and is constructed from GamaCoreMainSurvey by applying a strict  $r$ -band selection of  $r_{\text{pet}} < 19.4$  mag in G09 & G15 and  $r_{\text{pet}} < 19.8$  mag in G12 (this is implemented by extracting objects with  $\text{SURVEY\_CLASS} > 5$ ). While the final GAMA survey is independently  $r$ ,  $z$  and  $K$  selected, a strict  $r$ -band cut is imposed because observations during year 1 were  $r$ -band limited only with the additional cuts coming in in years 2 and 3. Future releases involving year 2 and 3 data will therefore include  $z$  and  $K$  band selected samples. Selecting on  $\text{SURVEY\_CLASS} > 5$  yields a catalogue of 114441 objects spread across the three GAMA regions. Table A2 contains a list of the parameters being released at this time. Redshift information (i.e., quality, signal-to-noise etc.) are provided for all targets while the redshifts are only provided for year 1 observations above  $r_{\text{pet}} = 19.0$  mag (52324 objects) and for a deeper narrow strip in G12 with declination  $\delta = \pm 0.5^\circ$  to  $19.0 < r_{\text{pet}} < 19.8$  mag (7533 objects). These limits are chosen as they represent our year 1 spectroscopic targeting limits (see Figs 17, 18 & 21 left). The redshift release constitutes approximately 50 per cent (59479 objects; 41902 GAMA; 17577 pre-existing), of the entire GAMA dataset (or 32.7 per cent of the redshifts acquired by the GAMA team over the past three years). This dataset provides a clean, well defined,  $r$ -band selected sample suitable for scientific exploitation as shown by Fig. 17 and Fig. 18. Please note that redshifts outside the specified flux limits or collected after year 1 are currently denoted as  $Z_{\text{HELIO}} = -2$ . The redshift quality and signal-to-noise information refers to the final best spectrum held in GamaCoreMainSurvey providing advance information as to whether a reliable redshift exists in the larger database. Requests for individual redshifts for specific objects can be directed to: [gama@gama-survey.org](mailto:gama@gama-survey.org)

### 6.3 GamaCoreAtlasSV — Available 2010-06-25

The GamaCoreAtlasSV is the subset of objects that have both a GAMA and H-ATLAS detection (see Smith et al. 2010 for details of source matching). 1175 objects coexist between the two data sets in a region defined by the geomet-

**Table 3.** The SURVEY\_CLASS parameter given in GamaTiling. Objects take the higher value if satisfying more than one criteria. All objects with SURVEY\_CLASS  $\geq 2$  pass the standard star-galaxy separation. See Baldry et al. (2010) for details.

| value | number | frac. $Q \geq 3$ | criteria and notes  |
|-------|--------|------------------|---|
| 7     | 59756  | 0.995            | $r_{\text{pet}} < 19.0$ and $\Delta_{\text{sg}} > 0.25$ (high priority in Year 1)                       |
| 6     | 54685  | 0.968            | $r_{\text{pet}} < 19.4$ or $r_{\text{pet}} < 19.8$ in G12 ( $\geq 6$ for $r$ -limited Main Survey)      |
| 5     | 1386   | 0.703            | $z_{\text{model}} < 18.2$ ( $\geq 5$ for SDSS-mag limited Main Survey)                                  |
| 4     | 3951   | 0.879            | $K_{\text{AB}} < 17.6$ ( $\geq 4$ for Main Survey)  |
| 3     | 33134  | 0.343            | $19.4 < r_{\text{pet}} < 19.8$ in G09 or G15 (F2 fillers)   |
| 2     | 14861  | 0.196            | $g_{\text{model}} < 20.6$ or $r_{\text{model}} < 19.8$ or $i_{\text{model}} < 19.4$ in G12 (F3 fillers) |
| 1     | 1255   | 0.577            | radio selected targets (F1 fillers, Ching et al. in preparation)  |
| 0     | 822    | 0.394            | $2 \leq \text{VIS\_CLASS} \leq 4$ or fails star-galaxy separation for $r_{\text{fib}} < 17$             |

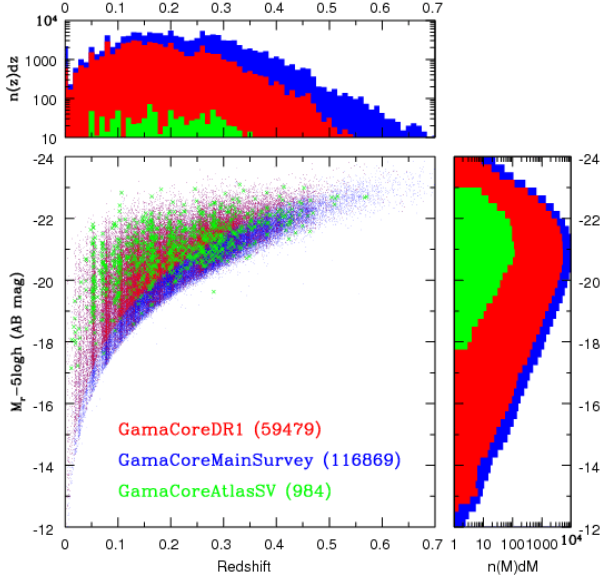


**Figure 23.** (Main panel). The absolute magnitude versus redshift plane for the three science ready catalogues (as indicated). (left) the distribution collapsed in redshift, (upper) the distribution collapsed in absolute magnitude.

ric overlap between G09 and the H-ATLAS SV region (see Fig. 22), with an approximate area of  $\sim 16.7 \text{ deg}^2$ . Using the GamaCoreMainSurvey catalogue we find  $\sim 15$  per cent of GAMA Main Survey targets have a H-ATLAS source match. Of these matches 89 do not have any available redshift, 306 have SDSS redshifts, 792 have GAMA redshifts and 1 object has a 2SLAQ-QSO redshift. The GAMA redshifts comprise of 523 year 1 redshifts, 182 year 2 redshifts and 87 year 3 redshifts. There are no magnitude cuts imposed for GamaCoreAtlasSV and therefore 178 of these redshifts derive from GamaCoreExtra. Note that to extract a homogeneously selected sample one must trim this catalogue to  $r_{\text{pet}} < 19.4$  mag. Table A3 shows the parameters included in this catalogue.

#### 6.4 GamaCoreExtraDR1 — Available 2010-06-25

The GamaCoreExtra catalogue contains information on all objects for which redshifts are known but lie outside the GamaCoreDR1 selection limits. In effect GamaCoreExtra serves as a redshift dumping ground and when com-

bined with GamaCoreMainSurvey or GamaCoreDR1 provides a full record of all objects with known redshifts in the three GAMA regions. This will include pre-existing redshifts at faint magnitudes in the public domain (predominantly from QSO and LRG surveys), along with filler objects targeted during the GAMA campaign. The parameters included are identical to GamaCoreDR1 and therefore also described in Table A2. GamaCoreExtraDR1 is an identical copy of GamaCoreExtra except with the GAMA redshifts embargoed until a later release. GamaCoreExtra is highly inhomogeneous and volatile as additional redshifts come to light and essentially forms the starting point for any extension to the GAMA survey. Currently it contains  $\sim 16\text{k}$  galaxies of which  $\sim 0.5\text{k}$  are pre-existing and  $\sim 15.5\text{k}$  have been acquired during GAMA observations. Requests for access to individual redshifts or redshifts for specified sub-regions should be directed to: [gama@gama-survey.org](mailto:gama@gama-survey.org)

#### 6.5 Future plans

The three science ready catalogues described in the previous sections are shown in Fig. 23 in the Absolute  $r$ -band magnitude ( $M_r - 5 \log h$ ) versus redshift ( $z$ ) plane (main panel), along with the collapsed  $N(z)$  and  $N(M_r)$  distributions (upper and right panels respectively). The absolute magnitudes are calculated using  $k$ -corrections derived from the GAMA  $u$  to  $K$  photometry, and total throughput (including atmosphere) temperature adjusted filter transmission curves, and the KCORRECT software package (Blanton & Roweis 2007). The figure is intended to provide a rough indication of the parameter range being explored with  $L^*$  galaxies routinely detected to  $z \approx 0.3$  and objects as faint as  $M_r = -12$  mag being recovered at  $z > 0.01$ . In future papers we will explore more comprehensively the completeness of the initial input catalogue (GamaTiling) in the bivariate brightness distribution plane (BBD; Hill et al. 2010, in prep.) through a detailed BBD-analysis (see Driver et al. 2005), as well as through comparisons to deeper and higher spatial resolution data.

In the near term the GAMA team will be producing a number of extended data products or data management units (DMUs), which include: spectral line analysis via GANDALF/ppxf (Sarzi et al., 2006; Cappellari & Emsellem 2004) and stellar population model fits (Maraston 2005; Thomas, Maraston & Bender 2003), bulge-disc decomposition via GALFIT3, stellar masses and revised photometric-redshifts via INTEREST, environmental markers, and group catalogues. These data products will be outlined in more detail in our next data release later in the year (Liske et

al., 2010, in prep.). Within the next 3–5 years we expect to ingest additional datasets from GALEX, HERSCHEL, WISE, GMRT, VISTA, VST, and ASKAP as well as expand our core AAT programme to cover a larger area of  $\sim 400$  sq deg. to  $r_{\text{Sersic}} < 19.8$  mag. In due course DMUs on multiwavelength SED and HI modeling will provide dust mass/temperature measurements, and gas and dynamical mass measurements.

## 7 SUMMARY

The GAMA basic-data including GAMA and pre-GAMA spectra and redshifts, GAMA SWARP processed images in *ugrizYJHK*, *u* to *K* matched aperture photometry, corrections to total magnitudes are now available at: <http://www.gama-survey.org/>. GAMA Data Release 1 (GamaCoreDR1) data is publicly available via a downloads page immediately, and the full catalogue (GamaCoreMainSurvey) is available for use by the GAMA team and collaborators. In addition we make publicly available a catalogue (GamaCoreAtlasSV) including year-2 data for the H-Atlas Science Verification region, which form the basis for a number of H-Atlas Science Verification papers.

Data inspections tools, including a MySQL tool and direct data inspection toolkit, are provided and will be developed further in due course. The sum of year 1, 2, and 3 data constitutes GAMA Phase I, which is now complete having utilised archival data from the Sloan Digital Sky Survey, the UK Infrared Deep Sky Survey, and the NASA Extragalactic Database and an initial allocation of 66 nights of Anglo-Australian Telescope time. Value added data products will be released from January 1st 2011 and regularly thereafter. GAMA Phase II is now underway and aims to add in additional area coverage as well as to extend the depth of the survey. The community is encouraged and invited to contact the team for early access to GamaCoreMainSurvey. The contents of this catalogue are described in Table A2.

## ACKNOWLEDGMENTS

First and foremost we would like to thank the staff of the former Anglo-Australian Observatory (now Australian Astronomical Observatory), for the the smooth running of the telescope and AAOmega during these observations and the funding support we have received from the STFC and the ARC.

Funding for the SDSS and SDSS-II has been provided by the Alfred P. Sloan Foundation, the Participating Institutions, the National Science Foundation, the U.S. Department of Energy, the National Aeronautics and Space Administration, the Japanese Monbukagakusho, the Max Planck Society, and the Higher Education Funding Council for England. The SDSS Web Site is <http://www.sdss.org/>. The SDSS is managed by the Astrophysical Research Consortium for the Participating Institutions. The Participating Institutions are the American Museum of Natural History, Astrophysical Institute Potsdam, University of Basel, University of Cambridge, Case Western Reserve University, University of Chicago, Drexel University, Fermilab, the Institute for Advanced Study, the Japan Participation

Group, Johns Hopkins University, the Joint Institute for Nuclear Astrophysics, the Kavli Institute for Particle Astrophysics and Cosmology, the Korean Scientist Group, the Chinese Academy of Sciences (LAMOST), Los Alamos National Laboratory, the Max-Planck-Institute for Astronomy (MPIA), the Max-Planck-Institute for Astrophysics (MPA), New Mexico State University, Ohio State University, University of Pittsburgh, University of Portsmouth, Princeton University, the United States Naval Observatory, and the University of Washington.

The UKIDSS project is defined in Lawrence et al. (2007). UKIDSS uses the UKIRT Wide Field Camera (WFCAM; Casali et al, 2007). The photometric system is described in Hewett et al. (2006), and the calibration is described in Hodgkin et al. (2009). The pipeline processing and science archive are described in Irwin et al. (2009, in prep) and Hambly et al. (2008). We have used data from the 4th data release.

This research has made use of the NASA/IPAC Extragalactic Database (NED), which is operated by the Jet Propulsion Laboratory, California Institute of Technology, under contract with the National Aeronautics and Space Administration.

The Millennium Galaxy Catalogue consists of imaging data from the Isaac Newton Telescope and spectroscopic data from the Anglo Australian Telescope, the ANU 2.3m, the ESO New Technology Telescope, the Telescopio Nazionale Galileo and the Gemini North Telescope. The survey has been supported through grants from the Particle Physics and Astronomy Research Council (UK) and the Australian Research Council (AUS). The data and data products are publicly available from <http://www.eso.org/~jliske/mgc/> or on request from J. Liske or S.P. Driver.

Finally we would like to acknowledge the use of Topcat, Stilts, SExtractor, SWARP, PSFex, GALFIT3 and ALADIN astronomical software packages and the r data analysis package.

## APPENDIX A: GAMA CATALOGUES

The four principle GAMA catalogues formed at this time are: GamaTiling, GamaCoreMainSurvey, GamaCoreDR1 and GamaCore AtlasSv. The parameters contained in these catalogues and their explanations are showing in Tables. A1–A3 respectively.



Table A1. Parameters held in GamaTiling

| Column | Parameter        | Units                       | Definition  |
|--------|------------------|-----------------------------|---|
| 1      | GAMA_ID          | N/A                         | Unique six digit GAMA identifier linked to GAMAs original SDSS DR6 input cat  |
| 2      | SDSS_ID          | N/A                         | Sloan Identifier from SDSS DR6  |
| 3      | RA_J2000         | Degrees                     | RA taken from SDSS DR6  |
| 4      | DEC_J2000        | Degrees                     | Declination taken from SDSS DR6   |
| 5      | r_FIBREMAG       | AB mag                      | Fibre magnitude   |
| 6      | r_PETRO          | AB mag                      | Extinction corrected <i>r</i> -band Petrosian flux derived from SDSS DR6      |
| 7      | u_MODEL          | AB mag                      | Extinction corrected model <i>u</i> mag from SDSS DR6                         |
| 8      | g_MODEL          | AB mag                      | Extinction corrected model <i>g</i> mag from SDSS DR6                         |
| 9      | r_MODEL          | AB mag                      | Extinction corrected model <i>r</i> mag from SDSS DR6                         |
| 10     | i_MODEL          | AB mag                      | Extinction corrected model <i>i</i> mag from SDSS DR6                         |
| 11     | z_MODEL          | AB mag                      | Extinction corrected model <i>z</i> mag from SDSS DR6                         |
| 12     | NUM_GAMA_SPEC    | N/A                         | Number of spectra available for this object                                   |
| 13     | r_SB             | AB mag arcsec <sup>-2</sup> | SDSS Petro half-light <i>r</i> -band surface brightness                       |
| 14     | SG_SEP           | mag                         | SDSS r_psf-r_model star-galaxy separation parameter                           |
| 15     | SG_SEP_JK        | mag                         | GAMA AUTO J-K - f_lucus star-galaxy separation parameter                      |
| 16     | K_KRON_SELECTION | AB mag                      | Extinction corrected K magnitude used for selection (Old)                     |
| 17     | TARGET_FLAGS     | bit                         | bitwise target criteria (see gama website)                                    |
| 18     | SURVEY_CLASS     | N/A                         | Survey class (see Table 3)  |
| 19     | PRIORITY_CLASS   | N/A                         | Priority class (see gama website)   |
| 20     | NEIGHBOUR_CLASS  | N/A                         | Number of Main Survey neighbours within 40 arcseconds (see Fig. 19)           |
| 21     | MASK_IC_10       | N/A                         | Mask value 0.0 to 1.0 around <i>V</i> < 10 mag stars (see Baldry et al. 2010) |
| 22     | MASK_IC_12       | N/A                         | Mask value 0.0 to 1.0 around <i>V</i> < 12 mag stars (see Baldry et al. 2010) |
| 23     | VIS_CLASS        | N/A                         | Visual classification (see Baldry et al. 2010)                                |
| 24     | VIS_CLASS_USER   | N/A                         | Initials of visual classifier for VIS_CLASS                                   |

## REFERENCES

- Adelman-McCarthy J.K., et al., 2008, *ApJS*, 175, 297
- Allen P.D., Driver S.P., Graham A.W., Cameron E., Liske J., De Propriis R., 2006, *MNRAS*, 371, 2
- Abazajian K.N., et al., 2009, *ApJS* 182, 543
- Baldry I.K., et al., 2010, *MNRAS*, 404, 86
- Baldry I.K., Balogh M.L., Bower R.G., Glazebrook K., Nichol R.C., Bamford S.P., Budavari T., 2006, *MNRAS*, 373, 469
- Baugh C.M., et al., 2004, *MNRAS*, 351, 44
- Belokurov V., et al., 2006, *ApJ*, 642, 137
- Bell E.F., McIntosh D.H., Katz N., Weinberg M.D., 2003, *ApJS*, 149, 289
- Bell E.F., Phleps S., Somerville, R.S., Wolf, C., Borch A., Meisenheimer, K., 2006, *ApJ*, 652, 270
- Bertin E., Arnouts S., 1996, *A&AS*, 117, 393
- Bertin E., Mellier Y., Radovich M, Missonnier G, Didelon P, Morin B, 2002, in *ASP Conf. Proc on Astronomical Data Analysis Software and Systems* (Eds. David A. Bohlender, Daniel Durand & Thomas H. Handley), 281, 228
- Blanton M.R., Roweis, S., 2007, *AJ*, 113, 734
- Bower R.G., Benson A.J., Malbon R, Helley J.C., Frenk C.S., Baugh C.M., Cole S.G., Lacey C.G., 2006, *MNRAS*, 370, 645
- Canon R., et al., 2006, *MNRAS*, 372, 425
- Cameron E., Driver S.P., 2007, *MNRAS*, 377, 523
- Cappellari M., Emsellem E., 2004, *PASP*, 116, 138
- Choi Y-Y, Park Changbom, Vogeley M.S., 2007, *ApJ*, 638, 87
- Cole S., et al., 2005, *MNRAS*, 362, 505
- Colless M., et al., 2001, *MNRAS*, 328, 1039
- Colless M., et al., 2003, *arXiv:astro-ph/0306581*
- Collister A.A., Lahav O., 2004, *PASP*, 116, 345
- Cook M., Barausse E., Evoli C., Lapi A., Granato G.L., 2010, *MNRAS*, 402, 2113
- Croom S., Saunders W., Heald R., 2004, *AAO Newsletter*, 106, 12
- Croom S.M., Smith R.J., Boyle B.J., Shanks T., Miller L., Outram P.J., Loaring N.S., 2004, *MNRAS*, 349, 1397
- Croom S.M., et al., 2009, *MNRAS*, 392, 19
- De Lucia G., Springer V., White S.D.M., Croton D., Kauffmann G., 2006, *MNRAS*, 366, 499
- De Propriis R, Conselice C.J., Liske J., Driver S.P., Patton D.R., Graham A.W., Allen P.D., 2007, *ApJ*, 666, 212
- Driver, S.P., Liske J., Cross N.J.G., De Propriis R., Allen P.D., 2005, *MNRAS*, 360, 81
- Driver S.P., et al., 2006, *MNRAS*, 368, 414
- Driver S.P., Popescu C.C., Tuffs R.J., Liske J., Graham A.W., Allen P.D., De Propriis, R, 2007, *MNRAS*, 379, 1022
- Driver S.P., Popescu C.C., Tuffs R.J., Graham A.W., Liske J., Baldry I., 2008, *ApJ*, 678, 101
- Driver S.P., et al., 2009, *A&G*, 50, 12
- Driver S.P., Robotham A.S.G., 2010, *MNRAS*, in press (arXiv:1005.2538)
- Eales, S., et al., 2010, *PASP*, 122, 499
- Eke V.R., et al., 2004, *MNRAS*, 348, 866
- Falco E.E., et al., 1999, *PASP*, 111, 438
- Gadotti, D.A., 2009, *MNRAS*, 393, 1531
- Graham A.W., Driver S.P., 2005, *PASA*, 22, 118
- Guzzo L. et al., 2008, *Nature*, 451, 541
- Heavens, A., Panter B., Jimenez R., Dunlop J., 2004, *Nature*, 428, 625
- Hill, D., et al., 2010a, *MNRAS*, submitted
- Hill, D., Driver S.P., Cameron E.C., Cross N.J.G., Liske J., 2010b, *MNRAS*, 404, 1215
- Hopkins A.M., McClure-Griffiths N.A., Gaensler B.M., 2008, *ApJ*, 682, L13

**Table A2.** Parameters held in GamaCoreMainSurvey, GamaCoreDR1, GamaCoreExtraDR1.

| Column | Parameter       | Units   | Definition  |
|--------|-----------------|---------|---|
| 1      | GAMA_IAU_ID     | N/A     | Unique IAU identifier   |
| 2      | GAMA_ID         | N/A     | Unique six digit GAMA identifier linked to GAMAs original SDSS DR6 input cat  |
| 3      | SDSS_ID         | N/A     | Sloan Identifier from SDSS DR6  |
| 4      | RA_J2000        | Degrees | RA taken from SDSS DR6  |
| 5      | DEC_J2000       | Degrees | Declination taken from SDSS DR6   |
| 6      | r_PETRO         | AB mag  | Extinction corrected <i>r</i> -band Petrosian flux derived from SDSS DR6  |
| 7      | Z_HELIO         | N/A     | Helio-centric redshift ( $-2 =$ embargoed, $= -0.9$ if $nQ=1$ )   |
| 8      | Z_QUALITY       | N/A     | Confidence on redshift (Definite, $nQ=4$ , Reliable $nQ=3$ , Uncertain $nQ=2$ , Unknown $nQ=1$ , Not observed $nQ=99$ ) |
| 9      | Z_SOURCE        | N/A     | Origin of redshift 1=SDSS DR6, 2=2dFGRS, 3=MGC, 4=2SLAQ-LRG, 5=GAMA, 6=6dFGS, 7=UZC, 8=2QZ, 9=2SLAQ-QSO, 10=NED         |
| 10     | Z_DATE          | N/A     | Date of observation if $z\_SOURCE=5$ (i.e., GAMA), otherwise 99   |
| 11     | Z_SN            | N/A     | Mean <i>s/n</i> of spectrum if $z\_SOURCE=5$ (i.e., GAMA), otherwise 99   |
| 12     | Z_ID            | N/A     | Filename of best available spectrum.  |
| 13     | PHOT_SOURCE     | N/A     | Photometric source ( $rd = r$ -band defined, $sd =$ self-defined, see Hill et al. 2010a)                                |
| 14     | u_KRON          | AB mag  | Extinction <i>u</i> -band Kron magnitude derived from <i>r</i> -band aperture   |
| 15     | g_KRON          | AB mag  | Extinction <i>g</i> -band Kron magnitude derived from <i>r</i> -band aperture   |
| 16     | r_KRON          | AB mag  | Extinction <i>r</i> -band Kron magnitude derived from <i>r</i> -band aperture   |
| 17     | i_KRON          | AB mag  | Extinction <i>i</i> -band Kron magnitude derived from <i>r</i> -band aperture   |
| 18     | z_KRON          | AB mag  | Extinction <i>z</i> -band Kron magnitude derived from <i>r</i> -band aperture   |
| 19     | Y_KRON          | AB mag  | Extinction <i>Y</i> -band Kron magnitude derived from <i>r</i> -band aperture   |
| 20     | J_KRON          | AB mag  | Extinction <i>J</i> -band Kron magnitude derived from <i>r</i> -band aperture   |
| 21     | H_KRON          | AB mag  | Extinction <i>H</i> -band Kron magnitude derived from <i>r</i> -band aperture   |
| 22     | K_KRON          | AB mag  | Extinction <i>K</i> -band Kron magnitude derived from <i>r</i> -band aperture   |
| 23     | u_KRON_ERR      | AB mag  | <i>u</i> -band Kron magnitude error   |
| 24     | g_KRON_ERR      | AB mag  | <i>g</i> -band Kron magnitude error   |
| 25     | r_KRON_ERR      | AB mag  | <i>r</i> -band Kron magnitude error   |
| 26     | i_KRON_ERR      | AB mag  | <i>i</i> -band Kron magnitude error   |
| 27     | z_KRON_ERR      | AB mag  | <i>z</i> -band Kron magnitude error   |
| 28     | Y_KRON_ERR      | AB mag  | <i>Y</i> -band Kron magnitude error   |
| 29     | J_KRON_ERR      | AB mag  | <i>J</i> -band Kron magnitude error   |
| 30     | H_KRON_ERR      | AB mag  | <i>H</i> -band Kron magnitude error   |
| 31     | K_KRON_ERR      | AB mag  | <i>K</i> -band Kron magnitude error   |
| 32     | EXTINCTION_r    | AB mag  | Galactic magnitude extinction in <i>r</i> -band   |
| 33     | r_SERS_MAG_10RE | AB mag  | <i>r</i> -band Sérsic magnitude truncated at 10 half light radii  |

- Hopkins P., Hernquist L., Cox T.J., Di Matteo T., Robertson B., Springel V., 2006, *ApJS*, 163, 1
- Ilbert, O., et al., 2009, *ApJ* 690, 1236
- Johnston, S., et al., 2007, *PASA*, 24, 174
- Jones D.H., et al., 2004, *MNRAS*, 355, 747
- Jones D.H., et al., 2009, *MNRAS*, 399, 683
- Kirkpatrick J. D., et al., 1999, *ApJ*, 519, 802
- Kron R.G., 1980, *ApJS*, 43, 305
- Lah, P., et al., 2009, *MNRAS*, 399, 1447
- Lawrence A., et al., 2007, *MNRAS*, 379, 1599
- Lewis I.J., et al., 2002, *MNRAS*, 333, 279
- Lilly S.J., et al., 2007, *ApJS*, 172, 70
- Lupton R., Blanton M.R., Fekete G., Hogg D.W., O’Mullane W., Szalay A., Wherry N., 2004, *PASP*, 116, 133
- Maraston C., 2005, *MNRAS*, 362, 799
- Martin D.C., et al., 2005, *ApJ*, 619, 1
- Masters K.L., et al., 2010, 404, 792
- Merritt D., Graham A.W., Moore, B., Diemand J., Terzic, B., 2006, *AJ*, 132, 2685
- Meyer, M., et al., 2004, *MNRAS*, 350, 1195
- Nichol R.C., et al., 2006, *MNRAS*, 368, 1507
- Nieto-Santisteban M.A., Szalay A.S., Gray J., 2004, in *ASP Conf. Proc on Astronomical Data Analysis Software Systems* (Eds. Francois Ochsenbein, Mark G Allen & Daniel Egret), 314, 666
- Norberg P., et al., 2001, *MNRAS*, 328, 64
- Novak G.S., Faber S.M., Dekel A., 2006, *ApJ*, 637, 96
- Padmanabhan N., et al., 2008, *ApJ* 674, 1217
- Peng, C.Y., Ho L.C., Impey C.D., Rix H-W., 2010, *AJ*, 139, 2097
- Percival W.J., et al., 2001, *MNRAS*, 327, 1297
- Petrosian V., 1976, *ApJ*, 209, 1
- Pohlen M., Trujillo I., 2006, *A&A*, 454, 759
- Popescu C.C., Misiriotis A., Kylyafis N.D., Tuffs R.J., Fischera J., 2000, *A&A*, 362, 138
- Robotham A.S.G., et al., 2010, *PASA*, 27, 76
- Sarzi M., et al., 2006, *MNRAS*, 366, 1151
- Sérsic J.L., 1963, *BAAA*, 6, 41
- Sérsic J.L., 1968, in *Observatorio Astronomico*, (Publ: ESO)
- Shao Z., Xiao Q., Shen S., Mo H.J., Xia X. Deng Z., *ApJ*, 659, 1159
- Sharp, R., et al., 2006, in *SPIE proceedings on Ground-based and Airborne Instrumentation for Astronomy* (Eds. Ian S. McLean, Masanori Iye), 6269, 62690
- Sharp R., Parkinson H., 2010, *MNRAS*, in press (arXiv:1007.0648)
- Skrutskie M.F., et al., 2006, *AJ*, 131, 1163
- Smith, D.J.B., et al., 2010, *MNRAS*, submitted (arXiv:1007.5260)
- Spergel D., et al., 2003, *ApJS*, 148, 175
- Thomas D., Maraston C., Bender R., 2003, *MNRAS*, 339, 897

Table A3. Parameters held in GamaCoreAtlasSV

| Column | Parameter       | Units   | Definition  |
|--------|-----------------|---------|---|
| 1      | GAMA_IAU_ID     | N/A     | IAU certified GAMA ID   |
| 2      | GAMA_ID         | N/A     | Unique six digit GAMA identifier linked to GAMAs original SDSS DR6 input cat  |
| 3      | SDSS_ID         | N/A     | Sloan Identifier from SDSS DR6  |
| 4      | RA_J2000        | Degrees | RA taken from SDSS DR6  |
| 5      | DEC_J2000       | Degrees | Declination taken from SDSS DR6   |
| 6      | r_PETRO         | AB mag  | Extinction corrected $r$ -band Petrosian flux derived from SDSS DR6   |
| 7      | Z_HELIO         | N/A     | Heliocentric redshift ( $-0.9$ if $nQ=1$ )  |
| 8      | Z_QUALITY       | N/A     | Confidence on redshift (Definite, $nQ=4$ , Reliable $nQ=3$ , Uncertain $nQ=2$ , Unknown $nQ=1$ , Not observed $nQ=99$ ) |
| 9      | Z_SOURCE        | N/A     | Origin of redshift 1=SDSS DR6, 2=2dFGRS, 3=MGC, 4=2SLAQ-LRG, 5=GAMA, 6=6dFGS, 7=UZC, 8=2QZ, 9=2SLAQ-QSO, 10=NED         |
| 10     | Z_DATE          | N/A     | Date of observation if $z\_SOURCE=5$ (i.e., GAMA), otherwise 99   |
| 11     | Z_SN            | N/A     | Mean s/n of spectrum if $z\_SOURCE=5$ (i.e., GAMA), otherwise 99  |
| 12     | Z_ID            | N/A     | Filename of best available spectrum.  |
| 13     | PHOT_SOURCE     | N/A     | Photometric source (rd = $r$ -band defined, sd = self-defined, see Hill et al. 2010a)                                   |
| 14     | u_KRON          | AB mag  | Extinction $u$ -band Kron magnitude derived from $r$ -band aperture   |
| 15     | g_KRON          | AB mag  | Extinction $g$ -band Kron magnitude derived from $r$ -band aperture   |
| 16     | r_KRON          | AB mag  | Extinction $r$ -band Kron magnitude derived from $r$ -band aperture   |
| 17     | i_KRON          | AB mag  | Extinction $i$ -band Kron magnitude derived from $r$ -band aperture   |
| 18     | z_KRON          | AB mag  | Extinction $z$ -band Kron magnitude derived from $r$ -band aperture   |
| 19     | Y_KRON          | AB mag  | Extinction $Y$ -band Kron magnitude derived from $r$ -band aperture   |
| 20     | J_KRON          | AB mag  | Extinction $J$ -band Kron magnitude derived from $r$ -band aperture   |
| 21     | H_KRON          | AB mag  | Extinction $H$ -band Kron magnitude derived from $r$ -band aperture   |
| 22     | K_KRON          | AB mag  | Extinction $K$ -band Kron magnitude derived from $r$ -band aperture   |
| 23     | u_KRON_ERR      | AB mag  | $u$ -band Kron magnitude error  |
| 24     | g_KRON_ERR      | AB mag  | $g$ -band Kron magnitude error  |
| 25     | r_KRON_ERR      | AB mag  | $r$ -band Kron magnitude error  |
| 26     | i_KRON_ERR      | AB mag  | $i$ -band Kron magnitude error  |
| 27     | z_KRON_ERR      | AB mag  | $z$ -band Kron magnitude error  |
| 28     | Y_KRON_ERR      | AB mag  | $Y$ -band Kron magnitude error  |
| 29     | J_KRON_ERR      | AB mag  | $J$ -band Kron magnitude error  |
| 30     | H_KRON_ERR      | AB mag  | $H$ -band Kron magnitude error  |
| 31     | K_KRON_ERR      | AB mag  | $K$ -band Kron magnitude error  |
| 32     | EXTINCTION_r    | AB mag  | Galactic magnitude extinction in $r$ -band  |
| 33     | r_SERS_MAG_10RE | AB mag  | $r$ -band Sérsic magnitude truncated at 10 half light radii   |
| 34     | HATLAS_IAU_ID   | N/A     | H-ATLAS ID as specified by Smith et al. (2010)  |

Trimble V., Ceja, J.A., 2010, AN, 331, 338

York D.G., et al., 2000, AJ, 120, 1579

Watson F., Colless M.C., 2010, A & G, 51, 3.16

Wild, V., Hewett P.C., 2005, MNRAS, 358, 1083

Willman B., et al., 2005, ApJ, 626, 85